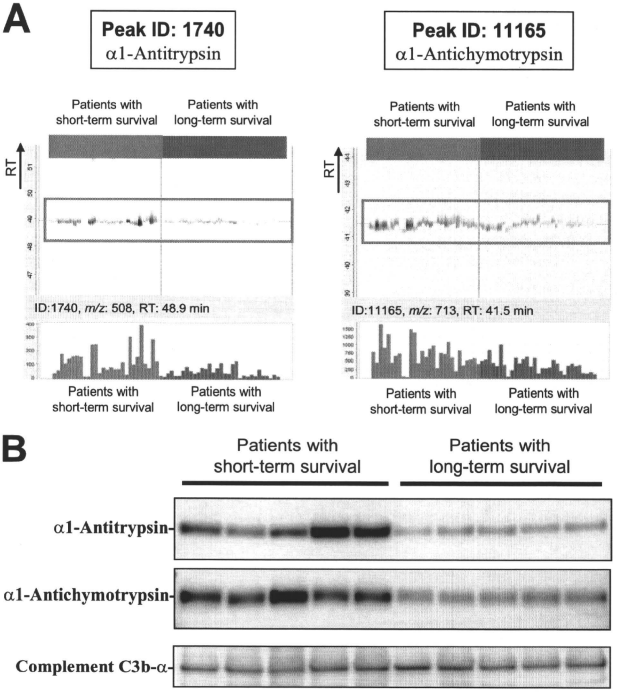

FIG. 2. *A*, representative MS peaks in 60 triplicate LC-MS runs (29 with short term survival (*red*) and 31 with long term survival (*blue*)) aligned along the retention time (*RT*) of LC. *Columns* represent the mean intensity of triplicates (*bottom*). *B*, detection of α_1-antitrypsin, α_1-antichymotrypsin, and complement C3b-α (loading control) by immunoblotting.

Reverse-phase Protein Microarray—Samples were serially diluted 1:500, 1:1,000, 1:2,000, and 1:4,000 using a Biomek 2000 Laboratory Automation Robot (Beckman Coulter) and randomly plotted onto ProteoChip® glass slides (Proteogen, Seoul, Korea) in quadruplicate in a 6,144-spot/slide format using a Protein Microarrayer Robot (Kaken Geneqs Inc., Matsudo, Japan). The spotted slides were incubated overnight with the same primary antibodies as those used in Western blotting. The slides were incubated with biotinylated anti-rabbit IgG (Vector Laboratories, Burlingame, CA) and subsequently with streptavidin-horseradish peroxidase conjugate (GE Healthcare). The peroxidase activity was detected using the Tyramide Signal Amplification (TSA®) Cyanine 5 System (PerkinElmer Life Sciences). The slides were counterstained with Alexa Fluor® 546-labeled goat anti-human IgG (Invitrogen) (spotting control).

The stained slides were scanned on a microarray scanner (InnoScan® 700AL, Innopsys, Carbonne, France). Fluorescence intensity, determined as the mean net value of quadruplicate samples, was determined using the Mapix® software package (Innopsys). All determined intensity values were transformed into logarithmic variables.

The reproducibility of reverse-phase protein microarray assay was revealed by repeating the same experiment. A plasma sample was serially diluted within a range of 1,024–16,384-fold. Each diluted sample was spotted in quadruplicate onto glass slides and blotted with anti-α_1-antitrypsin antibody. In a representative quality control experiment, the CC value was 0.977 between days, and the median CV was 0.026 among quadruplicate samples.

Statistical Analysis—Overall survival time was defined as the period from the date of starting gemcitabine monotherapy until the date of death from any cause or until the date of the last follow-up at which point the data were censored. We used the Kaplan-Meier method to plot overall survival curves. Statistical significance of intergroup differences was assessed with Welch's t test, Wilcoxon test, χ^2 test, or log rank test as appropriate. The maximally selected statistics (27) using the fitness of univariate Cox model (log likelihood) was used to determine which level (optimal cutoff point) of each factor best segregated patients in terms of survival.

Multivariate regression analysis was performed using ordinal Cox regression modeling. Factors included in the prediction model were selected with a forward stepwise selection procedure using Akaike's information criterion (AIC), and the result was confirmed using a backward stepwise procedure. The significance of differences between models with and without α_1-antitrypsin was assessed with the likelihood ratio test. The survival prediction model was internally validated by measuring both discrimination and calibration (28). Discrimination was evaluated using the concordance index, which is similar in concept to the area under the receiver operating characteristic curve. Calibration was evaluated with a calibration curve whereby patients are categorized by predicted survival and then

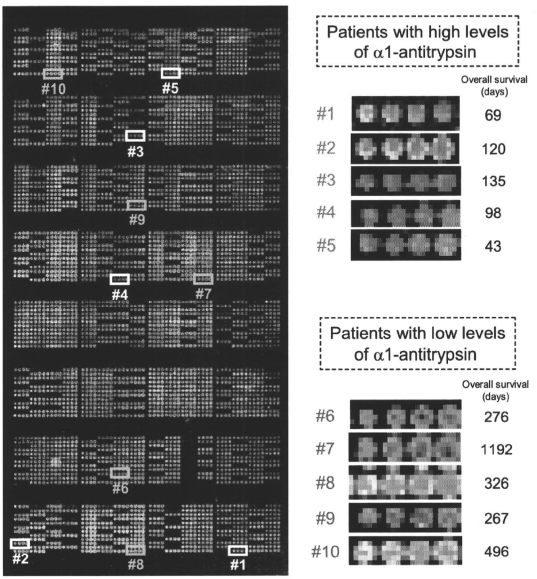

FIG. 3. *Left*, representative reverse-phase protein microarray slide stained with anti-α_1-antitrypsin antibody. *Right*, samples were randomly assigned, and quadruplicate spots of representative patients with high and low levels of α_1-antitrypsin were extracted.

plotted as actual *versus* predicted survival. Both discrimination and calibration were evaluated for the whole study cohort using 200 cycles of bootstrap resampling. Statistical analyses were performed using the open source statistical language R (version 2.7.0) with the optional module Design package.

RESULTS

The median survival estimate for the present study was 236 days (95% CI, 216–254 days), which is comparable to those of previous large scale studies (10, 22). To identify a prognostic factor in patients with advanced pancreatic cancer, we compared the base-line plasma proteome between 29 patients showing short term survival (<100 days) and 31 patients showing long term survival (>400 days) using 2DICAL. There was no significant difference in age, sex, body surface area, prior therapy, clinical stage, or gemcitabine pharmacokinetics (24) (Table I) between the two groups, but the patients with short term survival had significantly poorer base-line conditions such as liver function and Eastern Cooperative Oncology Group (ECOG) performance status than those with long term survival (Table I).

Among a total of 45,277 independent MS peaks detected within the range 250–1,600 *m/z* and within the time range of 20–70 min, we found that the mean intensity of triplicates differed significantly for 637 peaks ($p < 0.001$, Welch's *t* test). Fig. 1*A* is a representative two-dimensional view of all the MS peaks displayed with *m/z* along the *x axis* and the retention time of LC along the *y axis*. The 637 MS peaks whose expression differed significantly between patients with short term and long term survival are highlighted in *red*.

MS peaks that were increased in patients with short term survival with the highest statistical significance ($p = 2.57 \times 10^{-4}$) (Fig. 1*B*) matched the amino acid sequences of the α_1-antitrypsin (*AAT*) gene product (supplemental Fig. S1A). The MS peak with the second highest statistical significance ($p = 5.03 \times 10^{-4}$) was revealed to be derived from the α_1-antichymotrypsin (*AACT*) gene product (supplemental Fig. S1B). We calculated the false discovery rate (FDR) (29) and confirmed the significance of these MS peaks (FDR = 0.0327 for α_1-antitrypsin and FDR = 0.0428 for α_1-antichymotrypsin). Fig. 2*A* shows the distribution of the two peaks (ID 1740 (at 508 *m/z* and 48.9 min; α_1-antitrypsin) and ID 11165 (at 713 *m/z* and 41.5 min; α_1-antichymotrypsin)) in patients with short term (*red*) and long term survival (*blue*). The differential expression and identification of α_1-antitrypsin and α_1-antichymotrypsin were confirmed by denaturing SDS-PAGE and immunoblotting (Fig. 2*B*).

Correlation of α_1-Antitrypsin and α_1-Antichymotrypsin with Overall Survival—The relative levels of α_1-antitrypsin and α_1-antichymotrypsin in plasma or serum samples obtained from 304 patients with advanced pancreatic cancer prior to gemcitabine treatment (including 60 patients used in 2DICAL)

TABLE II

Univariate and multivariate Cox regression analyses of overall survival since the start of gemcitabine therapy (n = 304)

Factors except sex are regarded as continuous variables. A forward stepwise selection based on Akaike's information criterion was used to select parameters for multivariate analysis. p values of <0.050 are shown in bold. AST, aspartate aminotransferase; ALT, alanine aminotransferase; ALP, alkaline phosphatase.

	Univariate analysis		Multivariate analysis	
	Hazard ratio[a] (95% CI)	p	Hazard ratio[a] (95% CI)	p
Age (years)	0.99 (0.98–1.01)	0.380		
Female sex (*vs.* male)	1.07 (0.83–1.38)	0.610		
ECOG performance status	1.49 (1.22–1.80)	**<0.001**	1.36 (1.11–1.67)	**0.003**
Body surface area (m^2)	0.70 (0.33–1.50)	0.360		
Leukocytes	1.08 (1.05–1.11)	**<0.0001**	1.04 (1.00–1.08)	0.066
Platelets	1.07 (0.90–1.28)	0.450		
Hemoglobin (g/dl)	0.93 (0.85–1.01)	0.098		
Albumin (g/dl)	0.61 (0.45–0.82)	**0.001**		
Creatinine (mg/dl)	1.13 (0.60–2.14)	0.700		
AST (IU/liter)	1.01 (1.00–1.01)	**<0.001**		
ALT (IU/liter)	1.00 (1.00–1.01)	**0.033**		
ALP	1.09 (1.06–1.11)	**<0.0001**	1.07 (1.05–1.10)	**<0.0001**
α_1-Antitrypsin[b]	5.92 (3.09–11.37)	**<0.0001**	3.66 (1.89–7.11)	**0.0001**
α_1-Antichymotrypsin[b]	11.60 (2.69–50.01)	**0.001**		
Clinical stage IVa[c] (*vs.* IVb)	1.10 (0.85–1.38)	0.453		

[a] Hazard ratios are per 1,000/mm^3 increase for leukocytes, per 10 × 10^4/mm^3 increase for platelets, and per 100 units/liter increase for ALP. Hazard ratios for other continuous variables are per 1 unit increase for each variable.

[b] Logarithmic variable determined by reverse-phase protein microarray.

[c] According to Ref. 23.

were measured using reverse-phase protein microarrays (Fig. 3). Quadruplicate spots for representative patients with high and low levels of α_1-antitrypsin are shown in Fig. 3. There were no differences between plasma (n = 252) and serum (n = 52) with regard to the levels of α_1-antitrypsin and α_1-antichymotrypsin (plasma *versus* serum (mean ± S.D.): α_1-antitrypsin, 2.10 ± 0.19 *versus* 2.16 ± 0.16, p = 0.06; α_1-antichymotrypsin, 4.44 ± 0.10 *versus* 4.45 ± 0.08, p = 0.67).

Although the levels of α_1-antitrypsin and α_1-antichymotrypsin were not mutually correlated (Pearson's r = 0.274), either level showed a significant correlation with overall survival (Table II). When the most optimal cutoff value was determined by maximally selected analysis, the median survival time of patients with high levels of α_1-antitrypsin (>2.09 arbitrary units) was significantly shorter than that of patients with low levels (≤2.09) (201 days (95% CI, 176–219 days) *versus* 327 days (95% CI, 271–439 days), log rank $p = 2.26 \times 10^{-9}$; Fig. 4*A*). Similarly, the median survival time was significantly shorter in patients with α_1-antichymotrypsin levels of >4.41 (211 days (95% CI, 193 to 235 days)) than in those with levels of ≤4.41 (327 days (95% CI, 255–416 days)) ($p = 2.02 \times 10^{-4}$; Fig. 4*B*). Even when the 60 patients used for 2DICAL were excluded, the differences in survival separated by α_1-antitrypsin and α_1-antichymotrypsin levels were still significant (supplemental Fig. S2, A and B). However, the level of either α_1-antitrypsin or α_1-antichymotrypsin was not associated with tumor response (Spearman's ρ = 0.090 and ρ = 0.017, respectively). The increased level of α_1-antitrypsin in 58 patients who subsequently developed progressive diseases was statistically significant (p = 0.020; supplemental Fig. S3) but quite modest, confirming that it is not a predictive biomarker of tumor response.

Construction and Validation of Model Predicting Overall Survival Time—Univariate Cox regression analysis revealed that ECOG performance status and laboratory values including leukocyte count, albumin, aspartate aminotransferase, alanine aminotransferase, alkaline phosphatase, α_1-antitrypsin, and α_1-antichymotrypsin were correlated with overall survival of the 304 patients ($p < 0.05$; Table II). Because none of the parameters were able to predict survival outcome satisfactorily when used individually (data not shown), we attempted to construct a multivariate predictive model for estimation of overall survival. We searched for parameters using a forward stepwise selection procedure by AIC from all the clinical and laboratory data listed in Table II (available for all 304 cases) and found that a combination of α_1-antitrypsin, alkaline phosphatase, leukocyte count, and ECOG performance status provided the lowest AIC value. We also searched for parameters using a backward elimination algorithm and found that this identified the same combination of factors as that selected by a forward stepwise procedure. The base-line α_1-antitrypsin level was the second most significant contributor to the model (Table II). The prediction model using this combination of parameters was significantly compromised when the level of α_1-antitrypsin was excluded ($\Delta\chi^2 = 14.12$, $df = 1$, $p = 0.0002$, likelihood ratio test).

Based on the results of multivariate Cox regression analysis, we constructed a scoring system (nomogram) in which the values of the four parameters (α_1-antitrypsin, alkaline phosphatase, leukocyte count, and ECOG performance status) were integrated into a single score (total point) to estimate

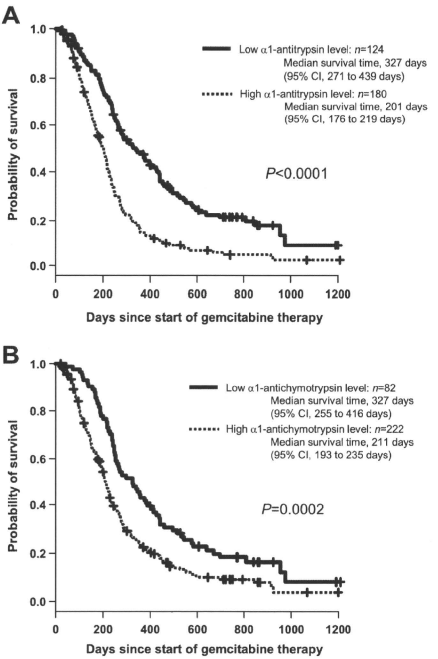

FIG. 4. **Kaplan-Meier plots of overall survival according to α_1-antitrypsin (*A*) and α_1-antichymotrypsin (*B*) levels.**

the survival outcome (Fig. 5*A*). The accuracy of the nomogram for prognostication was internally validated. The bootstrap-corrected concordance index was 0.672, and the calibration curve demonstrated good agreement between the predicted and observed outcomes (Fig. 5*B*). It was possible to estimate high risk patients by calculating the total points using the nomogram. The median survival time was 150 days (95% CI, 123–187 days) for patients with a total point score of >94 (n = 98) and 282 days (95% CI, 255–328 days) for patients with a score of ≤94 (n = 206), and the difference was significant ($p = 2.00 \times 10^{-15}$, log rank test; Fig. 5*C*). Even when the 60 patients used for 2DICAL analyses were excluded from the total points calculation, the difference was still significant ($p = 5.23 \times 10^{-10}$; supplemental Fig. S2*C*). The median survival time was 171 days (95% CI, 147–205 days) for patients with a score of >92 (n = 83) and 270 days (95% CI, 243–299 days) for patients with a score of ≤92 (n = 161). The cutoff value that optimally segregated patients into subgroups with a poor and good prognosis was determined by using the maximally selected statistics.

DISCUSSION

Currently, no diagnostic tool has been established for stratifying patients with advanced pancreatic cancer according to their likelihood of obtaining a survival benefit from gemcitabine treatment. Because some high risk patients may achieve prolonged survival through modification (or even withdrawal) of therapeutic protocols, a diagnostic method that can accurately identify such patients is necessary. We first compared the plasma proteome of two groups of patients who showed distinct clinical courses after receiving the same gemcitabine protocol (Fig. 1) and found that individuals who showed poor clinical courses had shown high base-line levels of plasma α_1-antitrypsin and α_1-antichymotrypsin (Figs. 1*B* and 2*A*). α_1-Antitrypsin is an abundant plasma protein that usually cannot be measured by MS. However, antibody-based protein depletion (30) allowed us to accentuate the differences in α_1-antitrypsin levels.

The results obtained by 2DICAL were then validated in a 5-fold larger cohort using a different methodology: high density reverse-phase protein microarray (Figs. 3 and 4 and Table II). Reverse-phase protein microarray is an emerging proteomics technology capable of validating new biomarkers because of its overwhelmingly high throughput (31, 32). Furthermore, reverse-phase protein microarrays require significantly smaller amounts of clinical samples for quantification than established clinical tests, such as ELISA. The prognostic significance of α_1-antitrypsin was further supported by multivariate survival analysis with stepwise covariate selection. The level of α_1-antitrypsin was selected as the second most significant factor following alkaline phosphatase (Table II), but α_1-antichymotrypsin was not selected. To derive clinical applicability from the above findings, we constructed a model (nomogram) including α_1-antitrypsin to estimate the survival period of pancreatic cancer patients (Fig. 5*A*), and its significance was internally validated (Fig. 5*B*). One previous study has demonstrated a correlation between an increased serum level of α_1-antitrypsin and short survival in patients treated surgically for pancreatic cancer (33). Although the number of cases examined was small (n = 44), the results support our present findings.

α_1-Antitrypsin and α_1-antichymotrypsin are members of the serine protease inhibitor (serpin) superfamily that plays key roles in the regulation of inflammatory cascades (34, 35). α_1-Antitrypsin and α_1-antichymotrypsin interact mainly with neutrophil elastase and neutrophil cathepsin G, respectively, and inhibit their protease activities (36). A protease-to-protease inhibitor imbalance in patients with genetic α_1-antitrypsin deficiency is reported to confer a higher risk of chronic pancreatitis (37). However, the serum level of α_1-antitrypsin in patients with pancreatic cancer varied significantly from case to case, and its clinical significance has remained unclear. We showed that increased concentrations of α_1-antitrypsin and α_1-antichymotrypsin in plasma/serum correlated with poor

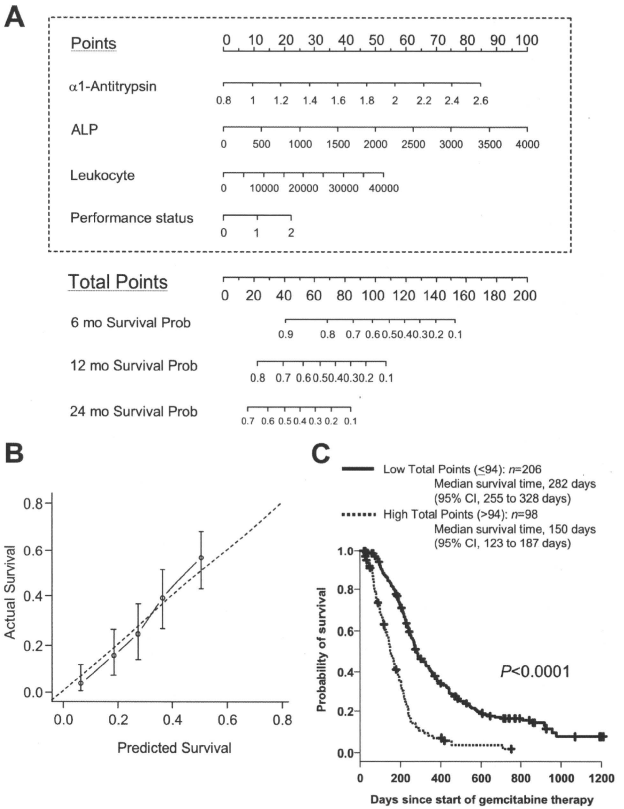

FIG. 5. *A*, nomogram for estimating the probability (*Prob*) of survival 6, 12, and 24 months (*mo*) after gemcitabine treatment. See supplemental Fig. S4 and its legend for details of usage. *B*, calibration curve demonstrating the correlation between predicted and actual survival at 12 months after gemcitabine treatment. *Bars* represent 95% CI. *C*, Kaplan-Meier plots of overall survival according to total points. *ALP*, alkaline phosphatase.

survival, indicating that patients with poor outcomes have lower base-line protease activities than those with favorable outcomes. How such a protease imbalance affects the progression of pancreatic cancer awaits further clarification in future studies.

In conclusion, we identified a prognostic biomarker potentially useful for selecting high risk patients with advanced pancreatic cancer who are unlikely to gain adequate survival benefit from the standard treatment. This may be of great clinical importance, especially when an alternative therapeutic option becomes available for patients with advanced pancreatic cancer in the future. However, the level of α_1-antitrypsin was not significantly correlated with the efficacy of gemcitabine, indicating that it may reflect the natural course of pancreatic cancer irrespective of treatment. Therefore, an independent prospective validation study will be definitely necessary to confirm the universality of the present findings. The absolute concentration of α_1-antitrypsin can be measured by nephelometry, but this measurement requires a larger sample volume than reverse-phase microarrays and for this reason could not be performed in this study. While bearing all these limitations in mind, the present findings may not only help to stratify patients with pancreatic cancer but also provide novel insights into the molecular mechanisms behind the malignant progression of this neoplasm, possibly leading to the development of novel therapeutic strategies.

Acknowledgments—We thank Ayako Igarashi, Tomoko Umaki, and Yuka Nakamura for technical assistance.

* This work was supported by the "Program for Promotion of Fundamental Studies in Health Sciences" conducted by the National Institute of Biomedical Innovation of Japan and the "Third-Term Comprehensive Control Research for Cancer" and "Research on Biological Markers for New Drug Development" conducted by the Ministry of Health and Labor of Japan.

S This article contains supplemental Figs. S1–S4 and Table S1.

¶ To whom correspondence should be addressed: Chemotherapy Division, National Cancer Center Research Inst., 5-1-1 Tsukiji, Chuo-ku, Tokyo 104-0045, Japan. Tel.: 81-3-3542-2511; Fax: 81-3-3547-6045; E-mail: jmatsuba@ncc.go.jp.

REFERENCES

1. Honda, K., Hayashida, Y., Umaki, T., Okusaka, T., Kosuge, T., Kikuchi, S., Endo, M., Tsuchida, A., Aoki, T., Itoi, T., Moriyasu, F., Hirohashi, S., and Yamada, T. (2005) Possible detection of pancreatic cancer by plasma protein profiling. *Cancer Res.* **65,** 10613–10622
2. American Cancer Society (2007) *Cancer Facts and Figures 2007*, pp. 16–17, American Cancer Society, Atlanta, GA
3. Ministry of Health, Labour and Welfare (2009) *Japanese Government: Vital Statistics of Japan*, Ministry of Health, Labour and Welfare, Tokyo
4. Rosewicz, S., and Wiedenmann, B. (1997) Pancreatic carcinoma. *Lancet* **349,** 485–489
5. Nieto, J., Grossbard, M. L., and Kozuch, P. (2008) Metastatic pancreatic cancer 2008: is the glass less empty? *Oncologist* **13,** 562–576
6. National Comprehensive Cancer Network (2009) *Clinical Practice Guidelines in Oncology: Pancreatic Adenocarcinoma*, Vol. 1, National Comprehensive Cancer Network, Fort Washington, PA
7. Burris, H. A., 3rd, Moore, M. J., Andersen, J., Green, M. R., Rothenberg, M. L., Modiano, M. R., Cripps, M. C., Portenoy, R. K., Storniolo, A. M., Tarassoff, P., Nelson, R., Dorr, F. A., Stephens, C. D., and Von Hoff, D. D. (1997) Improvements in survival and clinical benefit with gemcitabine as first-line therapy for patients with advanced pancreas cancer: a randomized trial. *J. Clin. Oncol.* **15,** 2403–2413
8. Matsubara, J., Ono, M., Negishi, A., Ueno, H., Okusaka, T., Furuse, J., Furuta, K., Sugiyama, E., Saito, Y., Kaniwa, N., Sawada, J., Honda, K., Sakuma, T., Chiba, T., Saijo, N., Hirohashi, S., and Yamada, T. (2009) Identification of a predictive biomarker for hematologic toxicities of gemcitabine. *J. Clin. Oncol.* **27,** 2261–2268
9. Stocken, D. D., Hassan, A. B., Altman, D. G., Billingham, L. J., Bramhall, S. R., Johnson, P. J., and Freemantle, N. (2008) Modelling prognostic factors in advanced pancreatic cancer. *Br. J. Cancer* **99,** 883–893
10. Louvet, C., Labianca, R., Hammel, P., Lledo, G., Zampino, M. G., André, T., Zaniboni, A., Ducreux, M., Aitini, E., Taïeb, J., Faroux, R., Lepere, C., and de Gramont, A. (2005) Gemcitabine in combination with oxaliplatin compared with gemcitabine alone in locally advanced or metastatic pancreatic cancer: results of a GERCOR and GISCAD phase III trial. *J. Clin. Oncol.* **23,** 3509–3516
11. Storniolo, A. M., Enas, N. H., Brown, C. A., Voi, M., Rothenberg, M. L., and Schilsky, R. (1999) An investigational new drug treatment program for patients with gemcitabine: results for over 3000 patients with pancreatic carcinoma. *Cancer* **85,** 1261–1268
12. Hanash, S. (2003) Disease proteomics. *Nature* **422,** 226–232
13. Yamaguchi, U., Nakayama, R., Honda, K., Ichikawa, H., Hasegawa, T., Shitashige, M., Ono, M., Shoji, A., Sakuma, T., Kuwabara, H., Shimada, Y., Sasako, M., Shimoda, T., Kawai, A., Hirohashi, S., and Yamada, T. (2008) Distinct gene expression-defined classes of gastrointestinal stromal tumor. *J. Clin. Oncol.* **26,** 4100–4108
14. Hayashida, Y., Honda, K., Osaka, Y., Hara, T., Umaki, T., Tsuchida, A., Aoki, T., Hirohashi, S., and Yamada, T. (2005) Possible prediction of chemoradiosensitivity of esophageal cancer by serum protein profiling. *Clin. Cancer Res.* **11,** 8042–8047
15. Taguchi, F., Solomon, B., Gregorc, V., Roder, H., Gray, R., Kasahara, K., Nishio, M., Brahmer, J., Spreafico, A., Ludovini, V., Massion, P. P., Dziadziuszko, R., Schiller, J., Grigorieva, J., Tsypin, M., Hunsucker, S. W., Caprioli, R., Duncan, M. W., Hirsch, F. R., Bunn, P. A., Jr., and Carbone, D. P. (2007) Mass spectrometry to classify non-small-cell lung cancer patients for clinical outcome after treatment with epidermal growth factor receptor tyrosine kinase inhibitors: a multicohort cross-institutional study. *J. Natl. Cancer Inst.* **99,** 838–846
16. Ono, M., Shitashige, M., Honda, K., Isobe, T., Kuwabara, H., Matsuzuki, H., Hirohashi, S., and Yamada, T. (2006) Label-free quantitative proteomics using large peptide data sets generated by nanoflow liquid chromatography and mass spectrometry. *Mol. Cell. Proteomics* **5,** 1338–1347
17. Negishi, A., Ono, M., Handa, Y., Kato, H., Yamashita, K., Honda, K., Shitashige, M., Satow, R., Sakuma, T., Kuwabara, H., Omura, K., Hirohashi, S., and Yamada, T. (2009) Large-scale quantitative clinical proteomics by label-free liquid chromatography and mass spectrometry. *Cancer Sci.* **100,** 514–519
18. Rocha Lima, C. M., Green, M. R., Rotche, R., Miller, W. H., Jr., Jeffrey, G. M., Cisar, L. A., Morganti, A., Orlando, N., Gruia, G., and Miller, L. L. (2004) Irinotecan plus gemcitabine results in no survival advantage compared with gemcitabine monotherapy in patients with locally advanced or metastatic pancreatic cancer despite increased tumor response rate. *J. Clin. Oncol.* **22,** 3776–3783
19. Van Cutsem, E., Vervenne, W. L., Bennouna, J., Humblet, Y., Gill, S., Van Laethem, J. L., Verslype, C., Scheithauer, W., Shang, A., Cosaert, J., and Moore, M. J. (2009) Phase III trial of bevacizumab in combination with gemcitabine and erlotinib in patients with metastatic pancreatic cancer. *J. Clin. Oncol.* **27,** 2231–2237
20. Heinemann, V., Quietzsch, D., Gieseler, F., Gonnermann, M., Schönekäs, H., Rost, A., Neuhaus, H., Haag, C., Clemens, M., Heinrich, B., Vehling-Kaiser, U., Fuchs, M., Fleckenstein, D., Gesierich, W., Uthgenannt, D., Einsele, H., Holstege, A., Hinke, A., Schalhorn, A., and Wilkowski, R. (2006) Randomized phase III trial of gemcitabine plus cisplatin compared with gemcitabine alone in advanced pancreatic cancer. *J. Clin. Oncol.* **24,** 3946–3952
21. Moore, M. J., Goldstein, D., Hamm, J., Figer, A., Hecht, J. R., Gallinger, S., Au, H. J., Murawa, P., Walde, D., Wolff, R. A., Campos, D., Lim, R., Ding, K., Clark, G., Voskoglou-Nomikos, T., Ptasynski, M., and Parulekar, W. (2007) Erlotinib plus gemcitabine compared with gemcitabine alone in patients with advanced pancreatic cancer: a phase III trial of the National Cancer Institute of Canada Clinical Trials Group. *J. Clin. Oncol.* **25,** 1960–1966
22. Herrmann, R., Bodoky, G., Ruhstaller, T., Glimelius, B., Bajetta, E., Schüller, J., Saletti, P., Bauer, J., Figer, A., Pestalozzi, B., Köhne, C. H., Mingrone, W., Stemmer, S. M., Tàmas, K., Kornek, G. V., Koeberle, D., Cina, S., Bernhard, J., Dietrich, D., and Scheithauer, W. (2007) Gemcitabine plus capecitabine compared with gemcitabine alone in advanced pancreatic cancer: a randomized, multicenter, phase III trial of the Swiss Group for Clinical Cancer Research and the Central European Cooperative Oncology Group. *J. Clin. Oncol.* **25,** 2212–2217
23. Japan Pancreas Society (ed) (2002) *General Rules for the Study of Pancreatic Cancer*, 5th Ed., Kanehara, Tokyo
24. Sugiyama, E., Kaniwa, N., Kim, S. R., Kikura-Hanajiri, R., Hasegawa, R., Maekawa, K., Saito, Y., Ozawa, S., Sawada, J., Kamatani, N., Furuse, J., Ishii, H., Yoshida, T., Ueno, H., Okusaka, T., and Saijo, N. (2007) Pharmacokinetics of gemcitabine in Japanese cancer patients: the impact of a cytidine deaminase polymorphism. *J. Clin. Oncol.* **25,** 32–42
25. Honda, K., Yamada, T., Hayashida, Y., Idogawa, M., Sato, S., Hasegawa, F., Ino, Y., Ono, M., and Hirohashi, S. (2005) Actinin-4 increases cell motility and promotes lymph node metastasis of colorectal cancer. *Gastroenterology* **128,** 51–62
26. Idogawa, M., Yamada, T., Honda, K., Sato, S., Imai, K., and Hirohashi, S. (2005) Poly(ADP-ribose) polymerase-1 is a component of the oncogenic T-cell factor-4/beta-catenin complex. *Gastroenterology* **128,** 1919–1936
27. Hothorn, T., and Zeileis, A. (2008) Generalized maximally selected statistics. *Biometrics* **64,** 1263–1269
28. Wang, S. J., Fuller, C. D., Kim, J. S., Sittig, D. F., Thomas, C. R., Jr., and Ravdin, P. M. (2008) Prediction model for estimating the survival benefit of adjuvant radiotherapy for gallbladder cancer. *J. Clin. Oncol.* **26,** 2112–2117
29. Storey, J. D., and Tibshirani, R. (2003) Statistical significance for genome-wide studies. *Proc. Natl. Acad. Sci. U.S.A.* **100,** 9440–9445
30. Huang, L., Harvie, G., Feitelson, J. S., Gramatikoff, K., Herold, D. A., Allen, D. L., Amunngama, R., Hagler, R. A., Pisano, M. R., Zhang, W. W., and Fang, X. (2005) Immunoaffinity separation of plasma proteins by IgY microbeads: meeting the needs of proteomic sample preparation and analysis. *Proteomics* **5,** 3314–3328
31. Grote, T., Siwak, D. R., Fritsche, H. A., Joy, C., Mills, G. B., Simeone, D.,

Whitcomb, D. C., and Logsdon, C. D. (2008) Validation of reverse phase protein array for practical screening of potential biomarkers in serum and plasma: accurate detection of CA19–9 levels in pancreatic cancer. *Proteomics* **8,** 3051–3060

32. Wulfkuhle, J. D., Liotta, L. A., and Petricoin, E. F. (2003) Proteomic applications for the early detection of cancer. *Nat. Rev. Cancer* **3,** 267–275
33. Trichopoulos, D., Tzonou, A., Kalapothaki, V., Sparos, L., Kremastinou, T., and Skoutari, M. (1990) Alpha 1-antitrypsin and survival in pancreatic cancer. *Int. J. Cancer* **45,** 685–686
34. Lomas, D. A., and Mahadeva, R. (2002) Alpha1-antitrypsin polymerization and the serpinopathies: pathobiology and prospects for therapy. *J. Clin. Investig.* **110,** 1585–1590
35. Stoller, J. K., and Aboussouan, L. S. (2005) Alpha1-antitrypsin deficiency. *Lancet* **365,** 2225–2236
36. Beatty, K., Bieth, J., and Travis, J. (1980) Kinetics of association of serine proteinases with native and oxidized alpha-1-proteinase inhibitor and alpha-1-antichymotrypsin. *J. Biol. Chem.* **255,** 3931–3934
37. Rabassa, A. A., Schwartz, M. R., and Ertan, A. (1995) Alpha 1-antitrypsin deficiency and chronic pancreatitis. *Dig. Dis. Sci.* **40,** 1997–2001

THE JOURNAL OF BIOLOGICAL CHEMISTRY VOL. 285, NO. 34, pp. 26289–26294, August 20, 2010

Traf2- and Nck-interacting Kinase Is Essential for Canonical Wnt Signaling in *Xenopus* Axis Formation*[S]

Received for publication, December 2, 2009, and in revised form, June 17, 2010 Published, JBC Papers in Press, June 21, 2010, DOI 10.1074/jbc.M109.090597

Reiko Satow[1], Miki Shitashige, Takafumi Jigami, Kazufumi Honda, Masaya Ono, Setsuo Hirohashi, and Tesshi Yamada

From the Chemotherapy Division, National Cancer Center Research Institute, 5-1-1 Tsukiji, Chuo-ku, Tokyo 104-0045, Japan

Wnt signaling pathways play important roles in various stages of developmental events and several aspects of adult homeostasis. Aberrant activation of Wnt signaling has also been associated with several types of cancer. We have recently identified Traf2- and Nck-interacting kinase (TNIK) as a novel activator of Wnt signaling through a comprehensive proteomic approach in human colorectal cancer cell lines. TNIK is an activating kinase for T-cell factor-4 (TCF4) and essential for the β-catenin-TCF4 transactivation and colorectal cancer growth. Here, we report the essential role of TNIK in Wnt signaling during *Xenopus* development. We found that *Xenopus TNIK* (*XTNIK*) was expressed maternally and that the functional knockdown of XTNIK by catalytically inactive XTNIK (K54R) or antisense morpholino oligonucleotides resulted in significant malformations with a complete loss of head and axis structures. XTNIK enhanced β-catenin-induced axis duplication and the expression of β-catenin-TCF target genes, whereas knockdown of XTNIK inhibited it. XTNIK was recruited to the promoter region of β-catenin-TCF target genes in a β-catenin-dependent manner. These results demonstrate that XTNIK is an essential factor for the transcriptional activity of the β-catenin-TCF complex and dorsal axis determination in *Xenopus* embryos.

Wnt signaling pathways are known to control both embryonic development and adult homeostasis. The canonical Wnt pathway is the best characterized among the Wnt signaling pathways and consists of a large number of factors. In short, secreted Wnt molecules are known to evoke downstream intracellular signaling events by binding to cell surface receptors, including the Frizzled family of proteins. These signals inhibit phosphorylation of β-catenin by glycogen synthase kinase 3β and subsequent degradation of β-catenin through the ubiquitin-proteasome system, resulting in the accumulation of cytoplasmic β-catenin protein. The accumulated β-catenin protein is then translocated into the nucleus, where it acts as a transcriptional co-activator by forming complexes with the T-cell factor (TCF)[2]/lymphoid enhancer factor (LEF) family of nuclear proteins. The β-catenin and TCF/LEF complexes have been shown to contain a variety of protein components that modulate transcriptional activity (1–5).

During *Xenopus* embryogenesis, the canonical Wnt pathway plays numerous important roles. It is well established that accumulation of β-catenin at the dorsal side of the embryo (referred to as "early" canonical Wnt signaling) induces organizer formation (6). In fact, down-regulation of β-catenin by antisense oligodeoxynucleotide or antisense morpholino oligonucleotides inhibits dorsal induction (7, 8). β-Catenin accumulation is dependent on dorsal enrichment of intracellular molecules including Dishevelled (Dsh) caused by cortical rotation that is triggered by sperm entry. Moreover, it has been shown that an extracellular ligand, maternal Wnt11, also asymmetrically activates the early canonical Wnt pathways (9). Early *Xenopus* embryos ubiquitously express three XTcf family members, *XTcf1*, *XTcf3*, and *XTcf4*, which are inherited by fertilized eggs as maternal transcripts. Maternal depletion of the XTcf genes has revealed their molecular functions. XTcf1 and XTcf3 have been shown to act cooperatively as repressors of dorsal genes including *Siamois* and *Xnr-3* in the ventral and lateral regions of early embryos in the absence of nuclear β-catenin accumulation, whereas XTcf1 and XTcf4 dorsally transactivate dorsal genes in cooperation with nuclear β-catenin (10, 11). The functional diversity of the XTcf genes may be due to differences in their DNA binding properties and binding co-factors. However, the mechanisms underlying these functions are yet to be precisely defined.

We and other researchers have recently identified that the germinal center kinase family protein, Traf2- and Nck-interacting kinase (TNIK) (12), comprised one component of the β-catenin-TCF4 complex (13, 14). TCF4 is a member of the TCF/LEF family implicated in intestinal epithelial cell renewal and colorectal carcinogenesis. We have revealed that TNIK phosphorylates TCF4 and activates the transcriptional activity of the β-catenin-TCF4 complex. Colorectal cancer cells were also shown to be highly dependent on the expression levels and kinase activity of TNIK for proliferation (15).

In the present study, we investigated the role of XTNIK during *Xenopus* embryogenesis. We show that XTNIK plays an essential role in β-catenin-mediated dorsal axis determination and transactivation.

* This work was supported by grants from the "Program for Promotion of Fundamental Studies in Health Sciences" conducted by the National Institute of Biomedical Innovation of Japan and the "Third-Term Comprehensive Control Research for Cancer" and "Research on Biological Markers for New Drug Development" conducted by the Ministry of Health, Labor, and Welfare of Japan.

[S] The on-line version of this article (available at http://www.jbc.org) contains supplemental Figs. S1–S5 and Tables S1 and S2.

[1] To whom correspondence should be addressed. Tel.: 81-3-3542-2511; Fax: 81-3-3547-6045; E-mail: resato@ncc.go.jp.

[2] The abbreviations used are: TCF, T-cell factor; LEF, lymphoid enhancer factor; MO, morpholino oligonucleotide; n-β-gal, nuclear β-gal; TNIK, Traf2- and Nck-interacting kinase; XTNIK, *Xenopus* TNIK; Xβ-catenin, *Xenopus* β-catenin.

EXPERIMENTAL PROCEDURES

Preparation of Xenopus Embryos—Preparation of *Xenopus laevis* embryos and microinjection were performed as described previously (16). Eggs were fertilized *in vitro* and dejellied with 1% sodium thioglycolate solution. Embryos were staged according to Nieuwkoop and Faber (17). Capped mRNA was synthesized by *in vitro* transcription (mMESSAGE mMACHINE kit; Ambion, Austin, TX).

Experiments were carried out according to the guidelines of the National Cancer Center Research Institute (Tokyo, Japan), which meet all the ethical requirements stipulated by Japanese law. The experimental protocols were reviewed and approved by the institutional ethics and recombination safety committees.

Real-time RT-PCR—Total RNA was isolated with TRIzol (Invitrogen). DNase-I-treated RNA was random-primed and reverse-transcribed using SuperScript II reverse transcriptase (Invitrogen). The TaqMan universal PCR master mix and custom TaqMan gene expression probe and primer sets were purchased from Applied Biosystems (Foster City, CA). The sequences of probe and primer sets were listed in supplemental Table S1. Amplification data measured as an increase in reporter fluorescence were collected using the PRISM 7000 sequence detection system (Applied Biosystems). mRNA expression levels relative to the internal control (ornithine decarboxylase (*odc*)) was calculated using the comparative threshold cycle (C_T) method (18).

Whole-mount in Situ Hybridization—Whole-mount *in situ* hybridization was performed according to Harland (19). Antisense and sense digoxigenin-labeled RNA probes were generated by *in vitro* transcription (MEGASCRIPT kit; Ambion) from linearized plasmids encoding *XTNIK*, *Xnr3*, *Siamois*, *chordin*, and *Xvent-1*. Injected embryos were traced by β-galactosidase staining with Red-Gal solution (Research Organics, Cleveland, OH) as described previously (15). The percentage of embryos showing unreduced expression at the Red-Gal staining region and the total number of examined embryos are indicated in supplemental Table S2.

Immunoblot Analysis—Protein samples were fractionated and immunoblotted as described previously (20). Anti-β-catenin (sc-7199), anti-Myc (9E10), anti-HA (12CA5), and anti-β-actin (AC-15) antibodies were purchased from Santa Cruz Biotechnology (Santa Cruz, CA), Zymed Laboratories Inc. (South San Francisco, CA), Abgent (San Diego, CA), and Abcam (Cambridge, MA), respectively.

Plasmids—pCS2-FLAG-*Xenopus* β-catenin (Xβ-catenin) (21) and -833pSia-Luc (22) were kindly provided by Dr. S. Sokol (Mount Sinai School of Medicine, New York, NY), and pCS2-nuclear β-gal (n-β-gal) (23, 24) was kindly provided by Drs. D. Turner, R. Rupp, and J. Lee (Fred Hutchinson Cancer Research Center, Seattle, WA). pCS2+-Myc and pCS2+-HA were kindly provided by Dr. M. Taira (University of Tokyo, Tokyo, Japan). pCS2+-Xnr5 (25) and pCS2+-BMP4-HA (26) were kindly provided by Dr. M. Asashima (University of Tokyo, Tokyo, Japan).

For the whole-mount *in situ* hybridization probes, partial sequences of *XTNIK*, *Xnr3*, *Siamois*, *chordin*, and *Xvent-1* were PCR-amplified using the following primer sets: *XTNIK*, 5′-aaagaaccctcctggaatgg-3′ and 5′-actgatctgttgtgggtctt-3′; *Xnr3*, 5′-ctatccaacctggaacatcctact-3′ and 5′-gaacagctttctggccaagac-3′; *Siamois*, 5′-tgccacgctgaaattattggg-3′ and 5′-gtggaaagtggttgctcttgg-3′; *chordin*, 5′-gttgttaaagggcttctatggg-3′ and 5′-gtctgccagttccataggac-3′; *Xvent-1*, 5′-ccaaccaaatatgccaaggaga-3′ and 5′-agccaccagggtaataaggg-3′. The amplified fragments were then subcloned into the EcoRV site of pcDNA3.1 (Invitrogen).

The 5′-UTR and ORF of LOC443633 (*XTNIK*), which are recognized by antisense morpholino oligonucleotide (MO) XTNIK-MO1 or -MO2, were PCR-amplified from the *X. laevis* IMAGE cDNA clone MXL1736-98358477 (Open Biosystems, Huntsville, AL) and subcloned into pCS2+-Myc (pCS-XTNIK-WT-Myc). The mutant form of pCS-XTNIK-WT-Myc (pCS-XTNIK-K54R-Myc) was constructed by mutagenesis with oligonucleotides 5′-AGGGTCATGGATGTCACAGGGG-ATG-3′ and 5′-AATAGCTGCAAGCTGTCCGGTTTT-AAC-3′ to alter the lysine 54 residue to arginine.

The ORF sequence of *XTNIK*, which is not recognized by XTNIK-MO1 or -MO2, was constructed by mutagenesis with oligonucleotides 5′-ATGGCcAGtGAtTCtCCGGCTCG-TAGCCTGGATGA-3′ (lowercase letters indicate modifications) and 5′-ATCGATGGGATCCTGCAAAAAGAACAA-3′ (pCS2-$XTNIK_{ORF}$-HA). *XTCF4* was PCR-amplified and subcloned into the EcoRV site of pCS2+-HA plasmid.

Antisense and Control MOs—The antisense MOs for *Xenopus TNIK* (XTNIK-MO1 and -MO2) and the corresponding control MOs (carrying five nucleotide substitutions (underlined nucleotides) within the XTNIK-MO1 and -MO2 sequences (5mis-Control-1 and -2, where "5mis" designates five mismatched nucleotides)) were obtained from Gene Tools (Philomath, OR). A database search confirmed the absence of a significant homologous sequence to the complements of XTNIK-MO1 and -MO2 in *X. laevis*. The sequences of the MOs used in this study were: XTNIK-MO1 (5′-GGG-AGTCGCTCGCCATGTTTCCTTT-3′), XTNIK-MO2 (5′-CCCCGTTCTTTCCACCTTGCGGCTG-3′), 5mis-Control-1 (5′-GGCAGTGGCTCCCCATCTTTCGTTT-3′), and 5mis-Control-2 (5′-CCGCGTTGTTTCGACCTTCCGCCTG-3′).

Luciferase Assay—Embryos were injected with -833pSia-Luc and pRL-TK plasmids (Promega, Madison, WI) with mRNA in the animal pole at the four-cell stage. Animal caps were dissected at stage 9, and luciferase activity was measured with the Dual-Luciferase reporter assay system (Promega) and normalized using *Renilla reniformis* luciferase activity as an internal control.

Chromatin Immunoprecipitation—Injected or uninjected embryos were fixed with 1% formaldehyde for 15 min at room temperature, washed twice with PBS, and lysed with radioimmune precipitation buffer lysis (Upstate Biotech Millipore, Lake Placid, NY) containing protease inhibitor mixture (Roche Diagnostics, Mannheim, Germany) and phosphatase inhibitor cocktails (Sigma-Aldrich) as reported previously (27). The solution was then sheared using a BioRuptor sonicator (Cosmo Bio Co., Tokyo, Japan) with 30-s pulses at 1-min intervals for 8 min at the maximum setting and then centrifuged with 14,000 × *g* at 4 °C for 10 min. The supernatant was diluted 10 times with ChIP dilution buffer (ChIP assay kit, Millipore, Billerica, MA), and 50 μl of the dilute was separated as the input sample. The

remainder was prewashed with protein A beads and incubated with 4 μg of anti-Myc antibody (9E10, Sigma) overnight at 4 °C. Immunoprecipitates were washed, and cross-links were removed according to the manufacturer's instructions (Millipore). Input and immunoprecipitated DNA were subjected to real-time PCR with probe/primers overlapping the promoter region of the *Xnr3* or *Siamois* gene. Immunoprecipitated DNA values relative to the input values was calculated using the comparative threshold cycle (C_T) method as mentioned previously (27).

Immunoprecipitation—Injected embryos were harvested at stage 10 and lysed with lysis buffer (0.5% Triton X-100, 250 mM NaCl, 50 mM Tris-HCl, pH 7.0) containing protease inhibitor mixture (Roche Diagnostics) and phosphatase inhibitor mixture (Sigma). After preclearing the lysates with mouse IgG-protein G complex, they were incubated with 4 μg of anti-Myc antibody (9E10), anti-HA antibody (H3663, Sigma), or normal mouse IgG overnight at 4 °C and precipitated with protein G-Sepharose (GE Healthcare, Buckinghamshire, UK).

Statistical Analysis—Results were obtained from at least three experiments, and statistical significance of the difference between groups was determined using Student's *t* test. Differences were considered significant for p values < 0.05.

RESULTS

Identification of Xenopus TNIK—A previously described registry has demonstrated the significant homology between human *TNIK* and *Xenopus XTNIK* in the UniGene *Xenopus laevis* database (termed hypothetical protein LOC443633). Although XTNIK lacks the portion equivalent to the C-terminal half of the human TNIK, the kinase domain spanning amino acids 25–289 was found to be highly conserved (98.9%) between human and *Xenopus* (supplemental Fig. S1).

We first examined the expression of *XTNIK* mRNA during *Xenopus* embryogenesis. We found that the expression of *XTNIK* was detected maternally. At the gastrula stages, zygotic *XTNIK* expression was observed and maintained until the tadpole stage (Fig. 1*A*). Whole-mount *in situ* hybridization demonstrated that *XTNIK* was ubiquitously expressed until the gastrula stage. At the neurula stage, localized expression was observed in the somatic mesoderm. In the tadpole stage, expression was localized to the somatic mesoderm, pronephros, branchial arches, eyes and otic vesicles (Fig. 1*B*).

Involvement of XTNIK in Dorsal Axis Determination—To examine the effects of TNIK and the catalytically inactive form of TNIK (K54R), we injected XTNIK or XTNIK (K54R) mRNA into *Xenopus* embryos. Injection of XTNIK (K54R) mRNA into dorsal blastomeres of eight-cell stage embryos inhibited the initiation of gastrulation at stage 10 (supplemental Fig. S2) and resulted in significant axis defects with a complete loss of head and axis structures (Fig. 2*A*). Injection of n-β-gal or XTNIK (WT) mRNA failed to affect axis formation (Fig. 2 and supplemental Fig. S2). Embryos injected with XTNIK or XTNIK (K54R) mRNA into the ventral blastomeres were also found to develop normally (data not shown). Consistent with the morphological defects, dorsal injection of TNIK (K54R) mRNA suppressed the expression of *Siamois*, *Xnr3*, and *chordin*, whereas dorsal injection of XTNIK (WT) increased the expression (Fig. 2, *B* and *C*, and supplemental Table S2). These

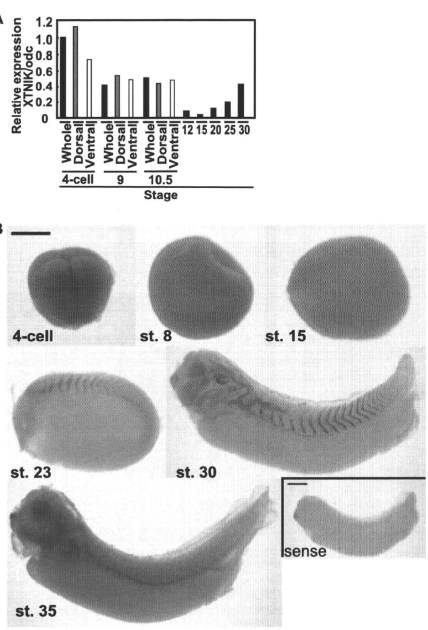

FIGURE 1. **Expression of *XTNIK* in *Xenopus* embryo.** *A*, expression of *XTNIK* was quantified using real-time PCR and expressed as a ratio relative to the expression of the ornithine decarboxylase (*odc*) gene. Embryos at the four-cell stage, stage 9, and stage 10.5 were divided into dorsal (*gray*) and ventral (*white*) sides. *B*, whole-mount *in situ* hybridization for the expression of *XTNIK*. Lateral views are presented. As a negative control, sense probe staining is presented in the *right bottom panel*. *Scale bars* = 0.5 mm. *st.*, stage.

results suggest involvement of XTNIK in dorsal axis determination in the *Xenopus* embryo.

XTNIK Enhanced β-Catenin-induced Secondary Axis Formation—We next examined whether XTNIK was involved in Wnt signaling. Co-injection of XTNIK (WT) mRNA with a low dose of Xβ-catenin (25 pg) into the ventral marginal zone of eight-cell stage embryos enhanced the formation of secondary axis with complete head structures. Catalytically inactive XTNIK (K54R) completely inhibited secondary axis formation (Fig. 3, *A* and *B*). The expression of *Xnr3*, *Siamois*, and *chordin* induced by ventral injection of Xβ-catenin was inhibited by XTNIK (K54R) (supplemental Fig. S3). Embryos injected with XTNIK (WT) or XTNIK (K54R) only (without Xβ-catenin) were found to develop normally (data not shown). These observations indicate that XTNIK enhances Wnt signaling in a β-catenin-dependent manner.

Translational Blockage of XTNIK Inhibits β-Catenin-induced Axis Formation—To block the translation of *XTNIK*, we designed two antisense MOs for *XTNIK* (namely MO1 and MO2), as well as their corresponding control MOs (5mis-Control-1 and -Control-2) in which five mismatched nucleotides

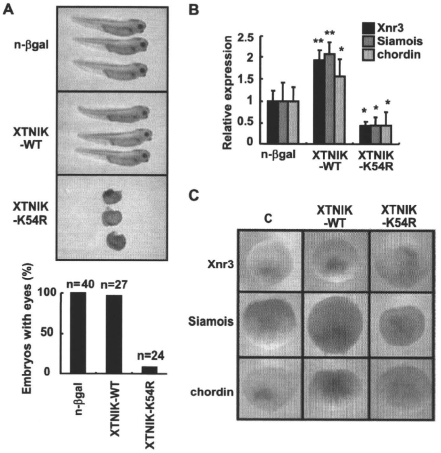

FIGURE 2. **XTNIK in dorsal axis determination.** mRNA for n-β-gal (500 pg), XTNIK-WT-Myc (500 pg), or XTNIK-K54R-Myc (500 pg) was injected into the dorsal marginal zone of eight-cell stage embryos. *A*, representative appearance of tadpoles and the ratio of tadpoles with eyes at stage 35. *B*, embryos were harvested at stage 9, and the relative mRNA expression of *Siamois*, *Xnr3*, and *chordin* was determined by real-time PCR. The statistical significance with respect to n-β-gal-injected control (*, $p < 0.05$; **, $p < 0.01$) was determined using Student's *t* test. *Bars* represent mean ± S.D. *C*, embryos were injected with XTNIK-WT-Myc (500 pg) or XTNIK-K54R-Myc (500 pg) together with n-β-gal (300 pg) mRNA at the four-cell stage and harvested at stage 9.5. The mRNA expression of *Xnr3*, *Siamois*, and *chordin* was examined by whole-mount *in situ* hybridization and stained blue. Red-Gal staining was used as a tracer. Dorsal views are presented.

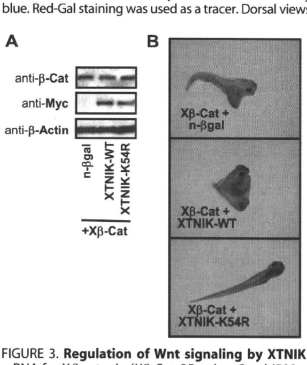

FIGURE 3. **Regulation of Wnt signaling by XTNIK in *Xenopus* embryos.** mRNA for Xβ-catenin (*Xβ-Cat*, 25 pg), n-β-gal (500 pg), XTNIK-WT-Myc (500 pg), or XTNIK-K54R-Myc (500 pg) was injected in the indicated combinations into the ventral marginal zone of eight-cell stage embryos. *A*, expression of Xβ-catenin, Myc-tagged XTNIK (WT or K54R), and β-actin (loading control) proteins was determined by immunoblotting. *B*, representative appearance of tadpoles and the ratio of tadpoles with secondary axis formation. *Complete* indicates axis formation with head-to-trunk structures. *Partial* indicates axis formation without heads. Secondary axes with or without cement glands were counted as complete or partial, respectively.

were inserted into the XTNIK-MO1 and -MO2 sequences, respectively. We found that XTNIK-MO1 and -MO2 blocked the translation of XTNIK-(WT)-Myc that contained the

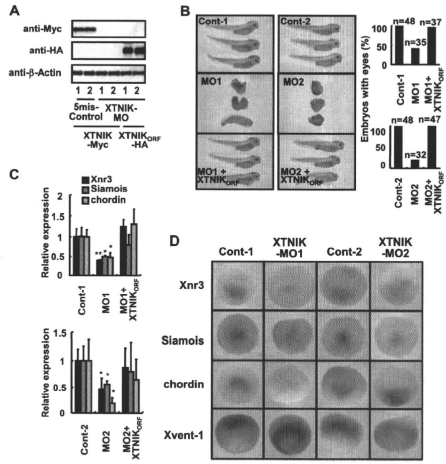

FIGURE 4. **Translational blockage of XTNIK inhibits dorsal axis formation.** 5mis-Control-1 (40 ng), 5mis-Control-2 (40 ng), XTNIK-MO1 (40 ng), or XTNIK-MO2 (40 ng) and XTNIK$_{ORF}$-HA (500 pg) mRNA were co-injected in the indicated combinations into the dorsal marginal zone of eight-cell stage embryos. *A*, expression of Myc-tagged XTNIK (WT), HA-tagged XTNIK$_{ORF}$, and β-actin (loading control) proteins was determined by immunoblotting. *B*, representative appearance of tadpoles and the ratio of tadpoles with eyes. *C*, relative mRNA expression of *Siamois*, *Xnr3*, and *chordin* at stage 9 was determined by real-time PCR. The statistical significance with respect to the control MO-injected control (*, $p < 0.05$; **, $p < 0.01$) was determined using Student's *t* test. *Bars* represent mean ± S.D. *D*, embryos injected with 5mis-Control-1 (40 ng), 5mis-Control-2 (40 ng), XTNIK-MO1 (40 ng), or XTNIK-MO2 (40 ng) together with n-β-gal (300 pg) mRNA at the four-cell stage and harvested at stage 9.5 (for *Xnr3*, *Siamois*, and *chordin*) or 10.5 (for *Xvent-1*). The mRNA expression of *Xnr3*, *Siamois*, *chordin*, and *Xvent-1* was examined by whole-mount *in situ* hybridization and stained blue. Red-Gal staining was used as a tracer. Dorsal views (*Xnr3*, *Siamois*, and *chordin*) and ventral-vegetal views (*Xvent-1*) are presented.

5′-UTR and ORF sequences recognized by the XTNIK-MO1 and -MO2 mRNA (Fig. 4*A*). Neither 5mis-Control-1 nor 5mis-Control-2 blocked this translation. Translation of HA-tagged XTNIK$_{ORF}$ (XTNIK$_{ORF}$-HA) mRNA (ORF of LOC443633 (*XTNIK*) lacking the 5′-UTR targeted by XTNIK-MO1 and -MO2) was not blocked by either XTNIK-MO1 or XTNIK-MO2. Therefore, we used XTNIK$_{ORF}$-HA for the rescue of XTNIK protein level reduced by XTNIK-MO1 and -MO2 in the following experiments.

We found that embryos injected dorsally with XTNIK-MOs (MO1 and MO2) failed to initiate gastrulation at stage 10 (supplemental Fig. S4) and developed into abnormal tadpoles with significantly reduced head and axis structures (Fig. 4*B*). Embryos injected with control MOs developed normally. The defects caused by XTNIK-MO were rescued by co-injection with XTNIK$_{ORF}$-HA (Fig. 4*B* and supplemental Fig. S4). The expression of *Siamois*, *Xnr3*, and *chordin* was also reduced by XTNIK-MO (Fig. 4, *C* and *D*, and supplemental Table S2), and the expression was reversed by co-injection with XTNIK$_{ORF}$-HA (Fig. 4*C*). Ventral injection of XTNIK-MO did not affect *Xvent-1* expression (Fig. 4*D*) and dorsal marker expression (data not shown).

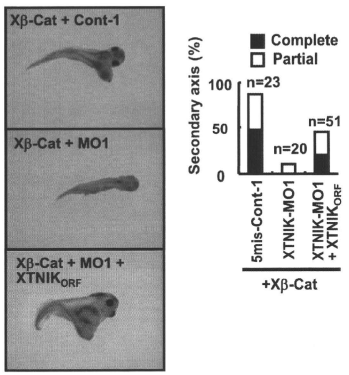

FIGURE 5. **Translational blockage of XTNIK inhibits β-catenin-induced secondary axis formation.** 5mis-Control-1 (40 ng), XTNIK-MO1 (40 ng), or XTNIK$_{ORF}$-HA (500 pg) mRNA and Xβ-catenin (*Xβ-Cat*) mRNA (50 pg) were co-injected in the indicated combinations into the ventral marginal zone of eight-cell stage embryos. The representative appearance of tadpoles and the ratio of tadpoles with secondary axis formation are shown. *Complete* indicates axis formation with head-to-trunk structures. *Partial* indicates axis formation without heads. Secondary axes with or without cement glands were counted as complete or partial, respectively.

XTNIK-MO1 and -MO2, but not their corresponding control MOs, blocked secondary axis formation induced by Xβ-catenin when co-injected into the ventral marginal zone of eight-cell stage embryos. The blockage was abrogated by co-injection of XTNIK$_{ORF}$-HA mRNA (Fig. 5 and supplemental Fig. S5). These results suggest that endogenous XTNIK is essential for β-catenin-dependent axis formation.

XTNIK Is an Essential, Conserved Enhancer of Canonical Wnt Signaling—In the animal cap assay, injection of Xβ-catenin induced expression of known Wnt signaling target genes, including *Siamois* and *Xnr3*, and dorsal gene, *chordin*. Co-injection with XTNIK (WT) enhanced the expression of these genes, whereas XTNIK (K54R) or XTNIK-MO down-regulated their expression (Fig. 6, *A–C*). Consistent with this, XTNIK (WT) enhanced the luciferase activity promoted by the *Siamois* promoter (22), as well as by human TNIK (Fig. 6*D*), suggesting functional conservation. Furthermore, ChIP assay revealed that XTNIK was recruited to the promoter region of Wnt signaling target genes (*Xnr3* or *Siamois*) in a β-catenin-dependent manner (Fig, 6E), which has been suggested in mouse crypt (14). Neither overexpression nor knockdown of XTNIK affected the target gene expression induced by Xnr5 or BMP4 (Fig. 6, *F–I*), suggesting a specific role of XTNIK in Wnt signaling. Finally, we also confirmed the interaction between XTNIK and XTCF4 in *Xenopus* embryos (Fig. 6*J*). These results suggest an essential, conserved role of XTNIK in Wnt signaling.

DISCUSSION

Our previous study identified TNIK as one of the protein components of TCF4-containing complexes in the colorectal cancer cell lines DLD1 and HCT-116, which each have a

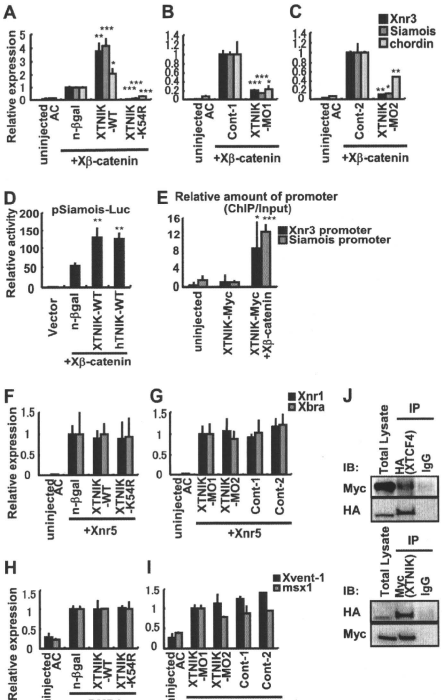

FIGURE 6. **XTNIK is an essential and specific enhancer for β-catenin-Tcf-transactivation.** *A–C*, mRNA for Xβ-catenin (25 pg), nuclear β-galactosidase (500 pg), XTNIK-WT-Myc (500 pg), XTNIK-K54R-Myc (500 pg), 5mis-Control-MO1 (*Cont-1*) (40 ng), XTNIK-MO1 (40 ng), 5mis-Control-MO2 (*Cont-2*) (40 ng), or XTNIK-MO2 (40 ng) was injected in the indicated combinations into the animal poles of four-cell stage embryos. Twenty animal caps (*AC*) per group were dissected at stage 9, cultured for 30 min, and harvested for RNA isolation. Relative mRNA expression of *Siamois*, *Xnr3*, and *chordin* was determined by real-time PCR. The statistical significance with respect to n-β-gal mRNA or control MO-injected controls (*, $p < 0.05$; **, $p < 0.01$; ***, $p < 0.001$) was determined using Student's *t* test. *D*, -833pSia-Luc plasmid (50 pg) and pRL-TK plasmid (10 pg) were co-injected with Xβ-catenin (25 pg), n-β-gal (500 pg), XTNIK (WT) (500 pg), or human TNIK (WT) (*hTNIK-WT*, 500 pg) mRNA in the indicated combinations into the animal poles of four-cell stage embryos. Ten animal caps per group were dissected at stage 9, cultured for 30 min, and harvested for the luciferase assay. The statistical significance with respect to the n-β-gal mRNA-injected control (**, $p < 0.01$) was determined using Student's *t* test. *E*, XTNIK-WT-Myc (500 pg) was injected with or without Xβ-catenin (100 pg) mRNA in the ventral marginal zone of embryos. Embryos were harvested at stage 10, and a ChIP assay was performed. *F–I*, mRNA for Xnr5 (5 pg), BMP4 (500 pg), nuclear β-galactosidase (500 pg), XTNIK-WT-Myc (500 pg), or XTNIK-K54R-Myc (500 pg) and for 5mis-Control-MO1 (*Cont-1*) (40 ng), XTNIK-MO1 (40 ng), 5mis-Control-MO2 (*Cont-2*) (40 ng), or XTNIK-MO2 (40 ng) was injected in the indicated combinations into the animal poles of four-cell stage embryos. Twenty animal caps per group were dissected at stage 9, cultured for 1.5 h, and harvested for RNA isolation. Relative mRNA expression of *Xnr1*, *Xbra*, *Xvent-1*, and *msx1* was determined by real-time PCR. *Bars* represent mean ± S.D. *J*, mRNA for XTNIK-WT-Myc (500 pg) and HA-XTCF4 (500 pg) was injected into the dorsal marginal zone of four-cell stage embryos and harvested at stage 9, and immunoprecipitation was performed.

respective truncating mutation in the *APC* gene and a missense mutation in the *CTNNB1* gene (12, 13). Recently, other investigators have also identified the presence of TNIK in TCF4-containing complexes in proliferative crypts of the murine small intestine (14). We and others have also demonstrated that TNIK interacts with and phosphorylates TCF4, in addition to activating transcription by the β-catenin-TCF4 complex. TNIK interacts with TCF4 through amino acids 1–289 and phosphorylates TCF4, whereas amino acids 100–215 of TCF4 are necessary for interaction with TNIK (15). The TCF4-interacting domain (amino acids 1–289) of human TNIK is highly conserved with XTNIK, sharing 99% identity. The TNIK-interacting domain (amino acids 100–215) of human TCF4 is also conserved in XTcf4 and XTcf3, which share 68 and 50% identity, respectively. These data indicate that the function of TNIK is most likely conserved between human and *Xenopus* in relation to TCF phosphorylation. In the current study, we showed that XTNIK interacted with XTCF4 and was essential for β-catenin-TCF-mediated transactivation and dorsal axis formation.

In early *Xenopus* embryo stages, three XTcf family members, XTcf1, XTcf3, and XTcf4, cooperatively regulate dorsal-ventral specification. XTcf1 and XTcf3 cooperatively act as repressors of β-catenin-TCF target genes by binding at the promoter region in the ventral region, whereas XTcf1 and XTcf4 transactivate β-catenin-TCF target genes in cooperation with nuclear β-catenin on the dorsal side (11). Considering the similarities between the TNIK-interacting domain of human TCF4 and the relevant domains of the XTcf genes, XTcf4 and XTcf3 are hypothesized to interact with, and be phosphorylated by, XTNIK. We demonstrated that dorsal inhibition of XTNIK by XTNIK (K54R) or XTNIK-MO suppresses dorsal axis formation and expression of β-catenin-TCF target genes. In contrast, ventral inhibition of XTNIK resulted in no obvious effects. When XTNIK (K54R) or XTNIK-MO was injected with β-catenin in the ventral marginal zone, β-catenin-induced secondary axis formation was blocked. These results suggest that XTNIK is not activated in the absence of nuclear β-catenin but is essential for β-catenin-mediated transactivation of its target genes. It has been reported that TNIK is recruited to the promoter region of its target genes in cooperation with TCF4 and β-catenin in a β-catenin-dependent manner (14). We also showed that XTNIK is recruited to the promoter region of the *Xnr3* and *Siamois* genes in a β-catenin-dependent manner. Taken together, our results suggest that the XTNIK promotes dorsal axis formation in cooperation with XTcf4 and β-catenin. These results demonstrate the conserved functional involvement of TNIK during canonical Wnt signaling *in vivo* and the essential function of TNIK for transactivation of β-catenin and TCF target genes. Aberrant activation of the Wnt pathway has been associated with several types of human cancers and disease. Thus, TNIK may prove useful as a therapeutic target molecule for specific inhibition of the Wnt signaling pathway for cancer therapeutics.

Acknowledgments—We thank Dr. S. Sokol (Mount Sinai School of Medicine, New York, NY) for providing pCS2+Xβ-catenin and -833pSia-Luc; Drs. D. Turner, R. Rupp, and J. Lee (Fred Hutchinson Cancer Research Center, Seattle, WA) for providing pCS2+n-β-gal; Dr. M. Taira (University of Tokyo, Tokyo, Japan) for providing pCS2+ vectors and for technical advice; and Dr. M. Asashima (University of Tokyo, Tokyo, Japan) for providing pCS2+-Xnr5 and pCS2+-BMP4-HA.

REFERENCES

1. Cavallo, R. A., Cox, R. T., Moline, M. M., Roose, J., Polevoy, G. A., Clevers, H., Peifer, M., and Bejsovec, A. (1998) *Nature* **395,** 604–608
2. Sun, Y., Kolligs, F. T., Hottiger, M. O., Mosavin, R., Fearon, E. R., and Nabel, G. J. (2000) *Proc. Natl. Acad. Sci. U.S.A.* **97,** 12613–12618
3. Sato, S., Idogawa, M., Honda, K., Fujii, G., Kawashima, H., Takekuma, K., Hoshika, A., Hirohashi, S., and Yamada, T. (2005) *Gastroenterology* **129,** 1225–1236
4. Idogawa, M., Masutani, M., Shitashige, M., Honda, K., Tokino, T., Shinomura, Y., Imai, K., Hirohashi, S., and Yamada, T. (2007) *Cancer Res.* **67,** 911–918
5. Shitashige, M., Hirohashi, S., and Yamada, T. (2008) *Cancer Sci.* **99,** 631–637
6. Moon, R. T., and Kimelman, D. (1998) *Bioessays* **20,** 536–545
7. Heasman, J., Crawford, A., Goldstone, K., Garner-Hamrick, P., Gumbiner, B., McCrea, P., Kintner, C., Noro, C. Y., and Wylie, C. (1994) *Cell* **79,** 791–803
8. Heasman, J., Kofron, M., and Wylie, C. (2000) *Dev. Biol.* **222,** 124–134
9. Tao, Q., Yokota, C., Puck, H., Kofron, M., Birsoy, B., Yan, D., Asashima, M., Wylie, C. C., Lin, X., and Heasman, J. (2005) *Cell* **120,** 857–871
10. Houston, D. W., Kofron, M., Resnik, E., Langland, R., Destree, O., Wylie, C., and Heasman, J. (2002) *Development* **129,** 4015–4025
11. Standley, H. J., Destrée, O., Kofron, M., Wylie, C., and Heasman, J. (2006) *Dev. Biol.* **289,** 318–328
12. Fu, C. A., Shen, M., Huang, B. C., Lasaga, J., Payan, D. G., and Luo, Y. (1999) *J. Biol. Chem.* **274,** 30729–30737
13. Shitashige, M., Satow, R., Honda, K., Ono, M., Hirohashi, S., and Yamada, T. (2008) *Gastroenterology* **134,** 1961–1971
14. Mahmoudi, T., Li, V. S., Ng, S. S., Taouatas, N., Vries, R. G., Mohammed, S., Heck, A. J., and Clevers, H. (2009) *EMBO J.* **28,** 3329–3340
15. Shitashige, M., Satow, R., Jigami, T., Aoki, K., Honda, K., Shibata, T., Ono, M., Hirohashi, S., and Yamada, T. (2010) *Cancer Res.* **70,** 5024–5033
16. Satow, R., Chan, T. C., and Asashima, M. (2002) *Biochem. Biophys. Res. Commun.* **295,** 85–91
17. Nieuwkoop, P. D., and Faber, J. (eds) (1956) *Normal Table of Xenopus laevis (Daudin): A Systematical and Chronological Survey of the Development from the Fertilized Egg till the End of the Metamorphosis,* North Holland Publishing Co., Amsterdam
18. Huang, L., Shitashige, M., Satow, R., Honda, K., Ono, M., Yun, J., Tomida, A., Tsuruo, T., Hirohashi, S., and Yamada, T. (2007) *Gastroenterology* **133,** 1569–1578
19. Harland, R. M. (1991) *Methods Cell Biol.* **36,** 685–695
20. Honda, K., Yamada, T., Hayashida, Y., Idogawa, M., Sato, S., Hasegawa, F., Ino, Y., Ono, M., and Hirohashi, S. (2005) *Gastroenterology* **128,** 51–62
21. Sokol, S. Y. (1996) *Curr. Biol.* **6,** 1456–1467
22. Fan, M. J., Grüning, W., Walz, G., and Sokol, S. Y. (1998) *Proc. Natl. Acad. Sci. U.S.A.* **95,** 5626–5631
23. Turner, D. L., and Weintraub, H. (1994) *Genes Dev.* **8,** 1434–1447
24. Rupp, R. A., Snider, L., and Weintraub, H. (1994) *Genes Dev.* **8,** 1311–1323
25. Takahashi, S., Yokota, C., Takano, K., Tanegashima, K., Onuma, Y., Goto, J., and Asashima, M. (2000) *Development* **127,** 5319–5329
26. Haramoto, Y., Tanegashima, K., Onuma, Y., Takahashi, S., Sekizaki, H., and Asashima, M. (2004) *Dev. Biol.* **265,** 155–168
27. Blythe, S. A., Reid, C. D., Kessler, D. S., and Klein, P. S. (2009) *Dev. Dyn.* **238,** 1422–1432

Cancer Research

Traf2- and Nck-Interacting Kinase Is Essential for Wnt Signaling and Colorectal Cancer Growth

Miki Shitashige[1], Reiko Satow[1], Takafumi Jigami[1], Kazunori Aoki[2], Kazufumi Honda[1], Tatsuhiro Shibata[3], Masaya Ono[1], Setsuo Hirohashi[1,3], and Tesshi Yamada[1]

Abstract

T-cell factor-4 (TCF4) is a transcription factor essential for maintaining the undifferentiated status and self-renewal of intestinal epithelial cells. It has therefore been considered that constitutive activation of TCF4 by aberrant Wnt signaling is a major force driving colorectal carcinogenesis. We previously identified Traf2- and Nck-interacting kinase (TNIK) as one of the proteins that interact with TCF4 in colorectal cancer cells, but its functional significance has not been elucidated. Here, we report that TNIK is an activating kinase for TCF4 and essential for colorectal cancer growth. TNIK, but not its catalytically inactive mutant, phosphorylated the conserved serine 154 residue of TCF4. Small interfering RNA targeting TNIK inhibited the proliferation of colorectal cancer cells and the growth of tumors produced by injecting colorectal cancer cells s.c. into immunodeficient mice. The growth inhibition was abolished by restoring the catalytic domain of TNIK, thus confirming that its enzyme activity is essential for the maintenance of colorectal cancer growth. Several ATP-competing kinase inhibitors have been applied to cancer treatment and have shown significant activity. Our findings suggest TNIK as a feasible target for pharmacologic intervention to ablate aberrant Wnt signaling in colorectal cancer. *Cancer Res; 70(12); 5024–33. ©2010 AACR.*

Introduction

The majority of colorectal cancers have somatic mutations in one of two genes involved in the canonical Wnt signaling pathway: the adenomatous polyposis coli (*APC*) and β-catenin (*CTNNB1*) genes. More than 80% of colorectal cancers show mutation of the *APC* gene (1), and half of the remainder have *CTNNB1* gene mutation (2, 3). Mutation of either gene causes failure of β-catenin degradation and accumulation of β-catenin protein (4–6). The accumulated β-catenin protein is translocated into the nucleus, where it forms complexes with T-cell factor (TCF)/lymphoid enhancer factor (LEF) family DNA-binding proteins and transactivates their target genes (7–9).

TCF4 is a member of the TCF/LEF family of transcription factors, which comprises LEF1 (*LEF1*), TCF1 (*TCF7*), TCF3 (*TCF7L1*), and TCF4 (*TCF7L2*; ref. 10). Among these factors, the aberrant activation of TCF4 by accumulated β-catenin has been implicated in colorectal carcinogenesis (11). TCF4 is commonly expressed in colorectal cancer cells (12). Physiologically, TCF4 is essential for maintaining the undifferentiated status of intestinal crypt epithelial cells. Mice lacking *Tcf7L2* show no proliferative compartment in the crypt regions (13). Induction of dominant-negative TCF4 restores epithelial cell polarity and converts colorectal cancer to a single layer of columnar epithelium (14), indicating that constitutive activation of TCF4 is necessary for maintaining the malignant phenotype.

Wnt signaling is a major force driving colorectal carcinogenesis, but not all the molecules mediating the signal can be drug targets. Restoration of the loss of function resulting from mutation of the *APC* gene is not realistic with current medical technology. We have therefore been searching for drug target molecules downstream of APC, especially in the nucleus (15). We previously identified 70 proteins present in the immunoprecipitate with anti-TCF4 antibody using highly tuned liquid chromatography and mass spectrometry (LC-MS; ref. 16). Among those proteins, Traf2- and Nck-interacting kinase (TNIK; ref. 17) attracted our interest because various small-molecule kinase inhibitors have been applied successfully to cancer treatment (18–20). Here, we report that colorectal cancer cells are highly dependent on the expression and kinase activity of TNIK for proliferation *in vitro* and *in vivo*. During the preparation of this article, Mahmoudi and colleagues also identified Tnik as a protein interacting with Tcf4 in the mouse intestinal crypt (21). Their data overlapped partly with ours: TNIK is an activating kinase for the TCF4 and β-catenin transcriptional complex. TNIK is a feasible target of pharmacologic intervention for manipulation of the aberrant Wnt signaling pathway.

Authors' Affiliations: [1]Chemotherapy Division, [2]Section for Studies on Host-Immune Response, and [3]Cancer Genomics Project, National Cancer Center Research Institute, Tokyo, Japan

Note: Supplementary data for this article are available at Cancer Research Online (http://cancerres.aacrjournals.org/).

Corresponding Author: Tesshi Yamada, Chemotherapy Division, National Cancer Center Research Institute, 5-1-1 Tsukiji, Chuo-ku, Tokyo 104-0045, Japan. Phone: 81-3-3542-2511; Fax: 81-3-3547-6045; E-mail: tyamada@ncc.go.jp.

doi: 10.1158/0008-5472.CAN-10-0306

Materials and Methods

Cell lines and antibodies

The human embryonic kidney cell line HEK293 and the human colorectal cancer cell line DLD1 were obtained from the Health Science Research Resources Bank. The human cervical cancer cell line HeLa was obtained from the Riken Cell Bank. The human colorectal cancer cell lines HCT-116 and WiDr were purchased from the American Type Culture Collection. The numbers of living cells were counted by trypan blue dye exclusion using a hemocytometer. Antibodies used in this study and their suppliers are listed in Supplementary Table S1.

Immunoprecipitation

Total cell lysates were prepared as described previously (16). The lysates were incubated at 4°C overnight with the indicated antibody or relevant control IgG and precipitated with Dynabeads protein G (Dynal Biotech).

Immunoblot analysis

Protein samples were fractionated by SDS-PAGE and blotted onto Immobilon-P membranes (Millipore). After incubation with the primary antibodies at 4°C overnight, the blots were detected with the relevant horseradish peroxidase–conjugated antimouse or antirabbit IgG antibody and enhanced chemiluminescence Western blotting detection reagents (GE Healthcare; ref. 22). Nuclear proteins were extracted using NE-PER Nuclear and Cytoplasmic Extraction Reagents (Pierce; ref. 22).

Immunohistochemistry

Fifty cases of sporadic colorectal cancer were selected from the pathology archive panel of the National Cancer Center Hospital (Tokyo, Japan). Immunoperoxidase staining was done using the avidin-biotin complex method (23).

Liquid chromatography and mass spectrometry

Protein bands in SDS-PAGE gels were visualized by Coomassie blue staining and digested using modified trypsin (Promega) as described previously (24). The tryptic peptides were concentrated and desalted with a 500-μm i.d. × 1 mm HiQ sil C18-3 trapping column (KYA Technologies). The peptides were then fractionated with a 0% to 80% acetonitrile gradient (200 nL/min for 1 hour) using a 150-μm i.d. × 5 cm C18W-3 separation column (KYA) and analyzed with a Q-Star Pulsar-*i* mass spectrometer equipped with a nanospray ionization source (Applied Biosystems). Reliability of protein identification was estimated by calculating the confidence value using ProID software (Applied Biosystems; ref. 16).

Plasmids

Human TNIK expression constructs [pCIneoHA-TNIK and its mutant (K54R); ref. 25] were kindly provided by Drs. M. Umikawa and K. Kariya (University of the Ryukyus, Okinawa, Japan). cDNA sequences encoding different parts of TNIK protein were subcloned into pBind (Promega). β-Catenin cDNA lacking the 134-amino-acid sequence in its NH_2 terminus was subcloned into pFLAG-CMV4 (Sigma-Aldrich; ref. 26). Full-length human TCF4 (splice form E) cDNA and its truncated forms were subcloned into pAct (Promega) or pFLAG-CMV4. The mutant form of TCF4, designated as TCF4S154A, was constructed with oligonucleotides GGCCCCATCACCGGCACACATTGTCTCTA and CGGGCATCCTTGAGGGCTTGTCTACTCTG to change the serine (S) 154 residue to alanine (A). Full-length human TCF4 and TCF4S154A cDNAs were subcloned into pEU-E01-MCS (CellFree Sciences). Dominant-negative TCF4, which lacks the NH_2-terminal β-catenin-binding site (TCF4DN; ref. 23), was subcloned into pcDNA3.1MycHis (Invitrogen). The cDNA sequence encoding amino acids 1–289 of TNIK, which is not recognized by small interfering RNA (siRNA) constructs 12 and 13 (see below), was subcloned into pCIneoHA (i.e., pCIneoHA-TNIKΔC) or an adenovirus shuttle plasmid pAdCMVloxP (ref. 27; pAdCMV-TNIKΔC).

Mammalian two-hybrid assay

Physical interactions between the TNIK and TCF4 proteins were assessed using the CheckMate Mammalian Two-Hybrid System (Promega) in accordance with the instructions provided by the supplier. HEK293 cells were cotransfected in triplicate with pBind, pAct, and pG5luc (Promega) plasmids using the Lipofectamine 2000 reagent (Invitrogen; refs. 24, 26).

Recombinant protein production

Glutathione *S*-transferase (GST) fusion proteins were synthesized using the ENDEXT Wheat Germ Expression Kit (CellFree Sciences). Hemagglutinin (HA)-tagged recombinant TNIK proteins were synthesized using rabbit reticulocyte lysate (TnT T7 Quick Coupled Transcription/Translation System, Promega).

RNA interference

Four siRNAs (CTNNB1-9, CTNNB1-11, TNIK-J-004542-12, and TNIK-J-004542-13) were synthesized and annealed by Dharmacon. Three nontargeting control RNAs (X, IX, and VIII) were purchased from Dharmacon.

The SureSilencing short hairpin RNA (shRNA) plasmids for human TNIK (pGeneClip-TNIK1, pGeneClip-TNIK2, and pGeneClip-TNIK3) and a negative control were purchased from SuperArray Bioscience.

Luciferase reporter assay

A pair of luciferase reporter constructs, TOP-FLASH and FOP-FLASH (Upstate), was used to evaluate TCF/LEF transcriptional activity. Cells were transiently transfected in triplicate with one of the luciferase reporters and phRL-TK (Promega; ref. 23). Luciferase activity was measured with the Dual-luciferase Reporter Assay System (Promega) and normalized using *Renilla reniformis* luciferase activity as an internal control (28). Data are presented as the ratio of TOP-FLASH to FOP-FLASH (TOP/FOP ratio).

Colony formation assay

Twenty-four hours after transfection, 400, 300, and 1,000 μg/mL G418 (Geneticin, Invitrogen) were added to the culture media of HeLa, DLD1, and HCT-116 cells, respectively. Cells were stained with Giemsa solution (Wako) after selection for 8 days (16).

Real-time reverse transcription-PCR

Total RNA was prepared with an RNeasy Mini Kit (Qiagen). DNase-I–treated RNA was random primed and reverse transcribed using SuperScript II reverse transcriptase (Invitrogen). The TaqMan Universal PCR master mix and predesigned TaqMan Gene Expression probe and primer sets were purchased from Applied Biosystems. Amplification data measured as an increase in reporter fluorescence were collected using the PRISM 7000 Sequence Detection system (Applied Biosystems). mRNA expression level relative to the internal control [β-actin (*ACTB*)] was calculated by the comparative threshold cycle (C_T) method (26).

Adenovirus vectors

The replication-incompetent recombinant adenovirus vectors were prepared by Cre/loxP-mediated recombination of a S360 adenoviral cosmid, which is an Ad 5 derivative with deletion of E1 and partial deletion of E3 (29), and the pAdCMVloxP or pAdCMV-TNIKΔC plasmid. The generated adenovirus vectors were designated AdCMV-Control and AdCMV-TNIKΔC, respectively. Cesium chloride–purified viruses were desalted by sterile Bio-Gel p-6 DG chromatography (Econopac DG 10, Bio-Rad) and diluted for storage in 13% glycerol/PBS solution. All viral preparations were confirmed to be free of $E1^+$ adenovirus by PCR assay (30).

Mouse experiments

HCT-116, DLD1, WiDr, or HeLa cells (5×10^6) suspended in 0.1 mL of PBS were s.c. inoculated into the flanks of 5-week-old female BALB/c nu/nu nude mice (SLC). One week later, the developed tumors were treated with siRNA together with atelocollagen (AteloGene, KOKEN). The final concentration of siRNA was 30 μmol/L and that of atelocollagen was 0.5%. A 0.2-mL volume of siRNA solution was injected directly into each tumor. siRNA remains intact *in vivo* for at least 1 week with the support of atelocollagen (31, 32). In some experiments, 5×10^8 pfu recombinant adenovirus vectors were coinjected. Tumor volume was determined as $V = AB^2\pi/6$, where A and B represent the largest and smallest dimensions, respectively (33). Mouse experiments were carried out according to the guidelines of the National Cancer Center Research Institute (Tokyo, Japan), which meet all the ethical requirements stipulated by Japanese law. The experimental protocols were reviewed and approved by the institutional ethics and recombination safety committees.

Results

TNIK is a component of the TCF4 and β-catenin complex

We analyzed the composition of proteins immunoprecipitated with anti-TCF4 antibody in two colorectal cancer cell lines (DLD1 and HCT-116) and identified TNIK (ref. 16; Supplementary Fig. S1). DLD1 has a truncating mutation in the *APC* gene and lacks the other allele, and HCT-116 has a missense mutation in the *CTNNB1* gene (2). TNIK was detected by immunoblotting of immunoprecipitates with anti-TCF4 or anti–β-catenin antibody, but not with control IgG. Conversely, β-catenin and TCF4 proteins were immunoprecipitated with anti-TNIK antibody (Fig. 1A). These results indicate that TCF4, β-catenin, and TNIK proteins form a complex in colorectal cancer cells. Two-hybrid assay revealed that TNIK interacted with TCF4 through amino acids 1–289, including the kinase domain (Fig. 1B). Amino acids 100–216 of TCF4 were necessary for interaction with TNIK (Fig. 1C).

Phosphorylation of TCF4 by TNIK

TCF4 protein was phosphorylated by TNIK (WT, wild-type; Fig. 2A–C), but not by the catalytically inactive mutant of TNIK with substitution (K54R) of the conserved lysine 54 residue in the ATP-binding pocket of the kinase domain (17). Tandem mass spectrometry (MS/MS) revealed that the serine 154 residue of TCF4 was phosphorylated by TNIK (WT) (Supplementary Fig. S2). Consistently, substitution of the serine 154 residue by alanine (S154A) abolished the phosphorylation of TCF4 by TNIK (Fig. 2C). The serine 154 residue of human TCF4 (*TCF7L2*) is conserved among species (Supplementary Fig. S3A) and shared with TCF3 (Supplementary Fig. S3B). TCF4 was phosphorylated on transfection of DLD1 cells with TNIK (WT), but not with TNIK (K54R) (Fig. 2D).

Nuclear translocation of TNIK

The catalytic activity of TNIK seems to be necessary for its nuclear translocation and interaction with TCF4 (Supplementary Fig. S4). DLD1 cells were transfected with HA-tagged TNIK (WT) or catalytically inactive TNIK (K54R) and analyzed by immunofluorescence microscopy (Supplementary Fig. S4A) and immunoprecipitation (Supplementary Fig. S4B). The wild-type TNIK was incorporated into the nuclei, whereas the K54R substitution significantly inhibited the nuclear translocation of TNIK (Supplementary Fig. S4A) and reduced the amount of TNIK interacting with TCF4 (Supplementary Fig. S4B).

The serine 764 (S764) residue of TNIK had been identified as a phosphorylation site by LC-MS/MS–based random sequencing of protein kinases (34), but its functional significance had remained unexplored. TNIK protein was distributed along the filamentous cytoskeleton (Supplementary Fig. S4C, anti-TNIK), whereas phosphorylated TNIK (anti-TNIKpS764) was detected mainly in the nuclei and colocalized with TCF4 (anti-TCF4).

Activation of TNIK by Wnt signaling

The phosphorylation and nuclear translocation of TNIK seem to be mediated, at least partly, through Wnt/β-catenin signaling (Fig. 3). TNIKpS764 was detected in colorectal cancer cells, but not in untransformed HEK293 cells (Fig. 3A). Transient transfection of HEK293 cells with β-catenin stabilized by deletion of the NH_2-terminal glycogen synthase kinase 3β phosphorylation site (β-cateninΔN134; ref. 26) induced the S764 phosphorylation and nuclear translocation of TNIK (Fig. 3B). Knockdown of β-catenin (*CTNNB1*) by siRNA (constructs 9 and 11) abolished the phosphorylation

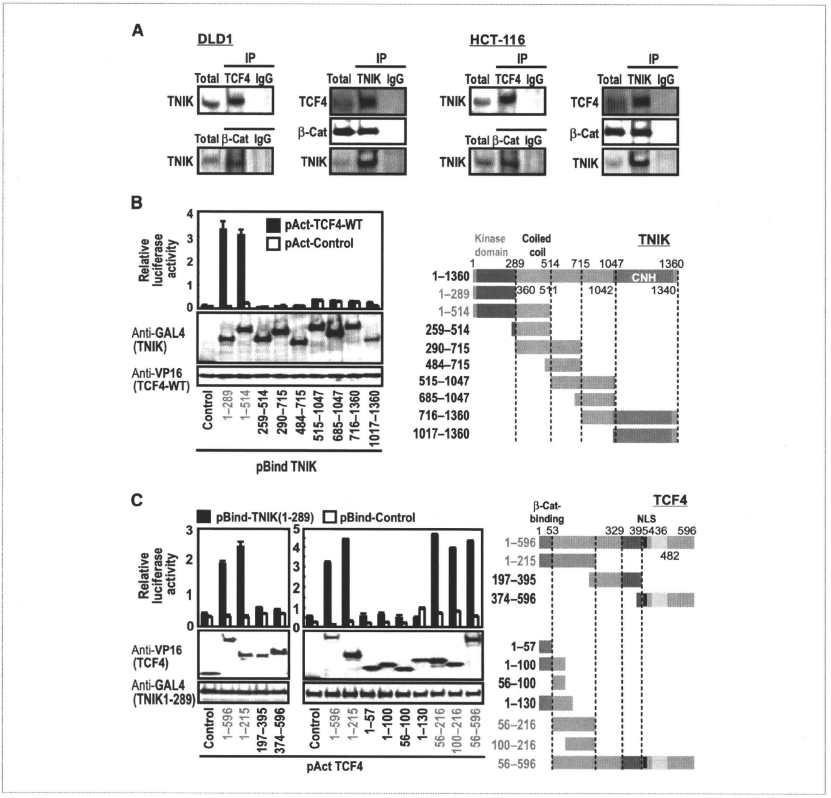

Figure 1. Interaction of TNIK with the TCF4 and β-catenin complex. A, total lysates (Total) and immunoprecipitates (IP) of DLD1 and HCT-116 cells with anti-TCF4, anti–β-catenin (β-cat), anti-TNIK antibody, or control IgG were blotted with the indicated antibodies. B, HEK293 cells were cotransfected with the pAct vector carrying the entire coding sequence of TCF4 cDNA (pAct-TCF4-WT, ■) or an empty vector (pAct-Control, □), the pBind plasmid carrying one of the serial deletion mutants of TNIK or an empty pBind vector (Control), and the pG5luc plasmid. C, HEK293 cells were cotransfected with the pBind vector carrying amino acids 1–289 of TNIK [pBind-TNIK(1–289), ■] or an empty vector [pBind-Control, □], the pAct plasmid carrying one of the truncated forms of TCF4 or an empty pAct vector (Control), and the pG5luc plasmid. B and C, the expression of constructs was confirmed by immunoblotting with anti-GAL4 (Bind) and VP16 (Act) antibodies. Forty-eight hours after transfection, luciferase activity was measured using *Renilla reniformis* luciferase activity as an internal control. Bars, SD. NLS, nuclear localization signal; CNH, citron homology.

and nuclear translocation of TNIK in colorectal cancer cells (Fig. 3C).

The expression of TNIK was examined in clinical specimens of colorectal cancer (Supplementary Fig. S5). Although the overall expression level of TNIK protein did not differ significantly between cancer and normal mucosa (Supplementary Fig. S5A and B), the expression of phosphorylated TNIK (pS764) was increased in cancer cells compared with neighboring normal intestinal epithelial cells (Supplementary Fig. S5C and D). Nuclear TNIKpS764 was detected most predominantly in the invasive front of colorectal cancer (Supplementary Fig. S5E), where β-catenin was accumulated in the nucleus and cytoplasm (Supplementary Fig. S5F).

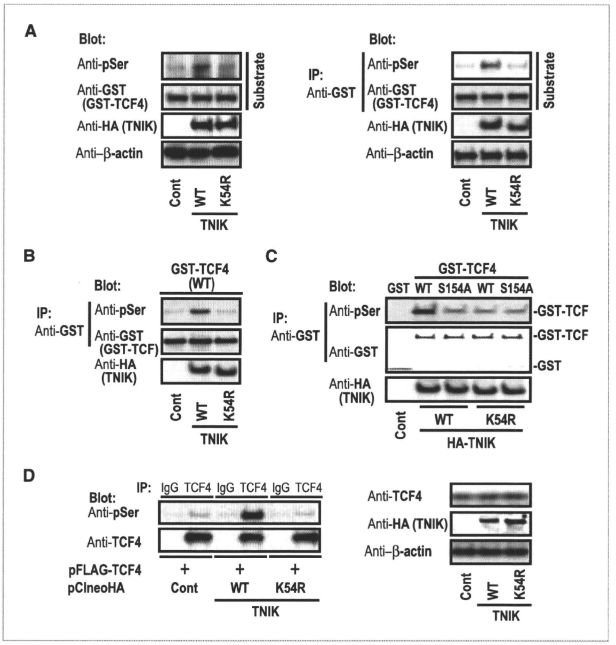

Figure 2. Phosphorylation of TCF4 by TNIK. A, HEK293 cells were transfected with pCIneoHA-TNIK-WT, pCIneoHA-TNIK-K54R, or empty plasmid (Cont). Twenty-four hours later, the comparable expression of TNIK proteins was confirmed by blotting with anti-HA and anti–β-actin antibodies. The immunoprecipitates (IP) with anti-HA antibody were incubated with GST-TCF4 recombinant protein at 30°C for 30 min in the presence of 0.1 mmol/L ATP and analyzed by blotting directly with anti-phosphoserine (pSer) and anti-GST antibodies (left) or by immunoprecipitation and blotting with the indicated antibodies (right). B and C, GST, GST-TCF4 (WT), and GST-TCF4 (S154A) proteins were incubated with the *in vitro* translation product of pCIneoHA-TNIK-WT, TNIK-K54R, or empty plasmid (Cont), immunoprecipitated with anti-GST antibody, and blotted with anti-pSer and anti-GST antibodies. The blots at the bottom (anti-HA) indicate the comparable production of TNIK-WT and TNIK-K54R proteins. D, DLD1 cells were transfected with pFLAG-TCF4 and pCIneoHA-TNIK-WT, TNIK-K54R, or empty plasmid. Immunoprecipitates with anti-TCF4 antibody or control IgG were blotted with the indicated antibodies (left). The expression of TCF4, TNIK, and β-actin (loading control) proteins was confirmed by immunoblotting (right).

Regulation of β-catenin–evoked transcriptional activity by TNIK

We then investigated the effects of TNIK on the transcriptional activity of the TCF4 and β-catenin complex (Supplementary Fig. S6). HeLa cells have wild-type *APC* and *CTNNB1* genes, and their TCF/LEF transcriptional activity is kept repressed (2, 35). Cotransfection with HA-tagged wild-type TNIK (WT), but not with TNIK (K54R), enhanced the β-cateninΔN134–evoked TCF/LEF transcriptional activity (Supplementary Fig. S6A). TNIK did not significantly affect transcriptional activity in the absence of β-cateninΔN134, indicating that the effects of TNIK are dependent on activation of Wnt signaling. Conversely, knockdown of TNIK by siRNA against TNIK (constructs 12 and 13) abolished the β-cateninΔN134–evoked TCF/LEF transcriptional activity (Supplementary Fig. S6B), which was also attenuated by an established inhibitor of Wnt signaling, dominant-negative TCF4 (TCF4DN; ref. 14). Knockdown of TNIK by shRNA against TNIK (constructs 1, 2, and 3) abolished the β-cateninΔN134–evoked colony formation, which was also inhibited by TCF4DN, but did not significantly affect the proliferation of HeLa cells that were not cotransfected with β-cateninΔN134 (Supplementary Fig. S6C).

TNIK is essential for colorectal cancer cell proliferation

Transient transfection with TNIK (WT), but not with TNIK (K54R), into DLD1 and HCT-116 cells also enhanced their TCF/LEF transcriptional activity (Supplementary Fig. S7A).

The effects were less remarkable, probably because endogenous TCF4 had already been activated by TNIK in these colorectal cancer cells. Then, substitution of the serine 154 residue of TCF4 by alanine (S154A) abolished the TNIK (WT)–induced TCF/LEF transcriptional activity (Supplementary Fig. S7B). Knockdown of TNIK suppressed the TCF/LEF transcriptional activity (Fig. 4A), proliferation (Fig. 4B), and colony formation (Fig. 4C) of DLD1 and HCT-116 cells. The expression of known target genes of the β-catenin and TCF/LEF complexes (36–40), such as axis inhibitor-2 (*AXIN2*), c-myc (*MYC*), c-jun (*JUN*), and matrilysin (*MMP7*), except for cyclin D1 (*CCND1*), was significantly reduced by transient transfection with siRNA against TNIK (Fig. 5). The siRNA-mediated reduction of transcriptional activity and cell proliferation was rescued by cotransfection with the kinase domain (amino acids 1–289) of TNIK (TNIKΔC), which lacks the sequences targeted by siRNAs (Supplementary Fig. S8).

Regression of established tumors after injection of siRNA against TNIK

We next examined the effects of TNIK on the growth of human colon cancer cells *in vivo* (Fig. 6). HCT-116 cells were implanted in the flanks of immunodeficient mice. One week after the inoculation, siRNA against TNIK (12 or 13) mixed with atelocollagen (31) was injected into the tumors (224.5 ± 8.9 mm^3). Three days after the siRNA injection, some tumors were excised, and the silencing of TNIK was confirmed by real-time PCR (Fig. 6A). The volume of xenografts was monitored for 18 days after siRNA injection (Fig. 6B). We found that the tumors regressed almost completely after an injection of siRNA against TNIK. Figure 6C and D shows the appearance of representative mice and excised tumors. Tumors treated with siRNA against TNIK (12 or 13) were significantly smaller than those that were untreated (No treat), treated with only atelocollagen (Atelo only), or treated with control RNA (X or IX; Fig. 6D). We observed similar regression of established tumors after an injection of siRNA against TNIK in two other colorectal cancer cell lines, DLD1 and WiDr (Supplementary Figs. S9 and S10), but not in Wnt-inactive HeLa cells (Supplementary Fig. S11). The siRNA-mediated reduction of tumor growth was rescued by coinjection of an adenovirus vector encoding the kinase domain of TNIK (TNIKΔC; Supplementary Fig. S12). The detection of cleaved poly(ADP-ribose) polymerase 1 (Supplementary Fig. S12B) indicated the induction of apoptosis by silencing of TNIK.

Discussion

The Wnt signaling pathway plays an important role in the maintenance of intestinal epithelial stem cell reservoirs. In fact, undifferentiated cells at the bottom of the intestinal crypts accumulate nuclear β-catenin (41). Mahmoudi and colleagues showed that TNIK interacted with and phosphorylated β-catenin as well as TCF4 (21). We further showed that TNIK phosphorylated the S154 residue of TCF4 (Fig. 2; Supplementary Fig. S2). The recombinant TCF4 protein was directly phosphorylated by the *in vitro* translation product of TNIK (Fig. 2B and C), and the effects of TNIK were compromised by substitution of the S154 residue of TCF4 (Fig. 2C). Substitution of the serine 154 residue of TCF4 by alanine (S154A) abolished the TNIK (WT)–induced TCF/LEF transcriptional activity of colon cancer cells (Supplementary Fig. S7B), indicating that the TNIK-mediated phosphorylation of the residue is essential for the transcriptional activity of TCF4. The serine residue of TCF4 is conserved from human to zebrafish and also in TCF3 (Supplementary Fig. S3), indicating the biological importance of its phosphorylation.

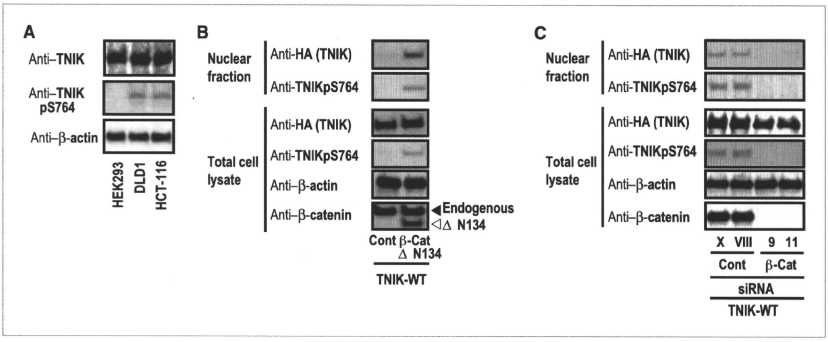

Figure 3. Activation of TNIK by Wnt signaling. A, immunoblotting of total lysates extracted from HEK293, DLD1, or HCT-116 cells with the indicated antibodies. B, HEK293 cells were cotransfected with pFLAG-β-cateninΔN134 (β-catΔN134) or empty plasmid (pFLAG-CMV4; Cont) and pCIneoHA-TNIK-WT. C, DLD1 cells were cotransfected with control RNA (X or VIII) or siRNA targeting β-catenin (9 or 11) and pCIneoHA-TNIK-WT. B and C, total cell lysates and nuclear fraction proteins were blotted with the indicated antibodies.

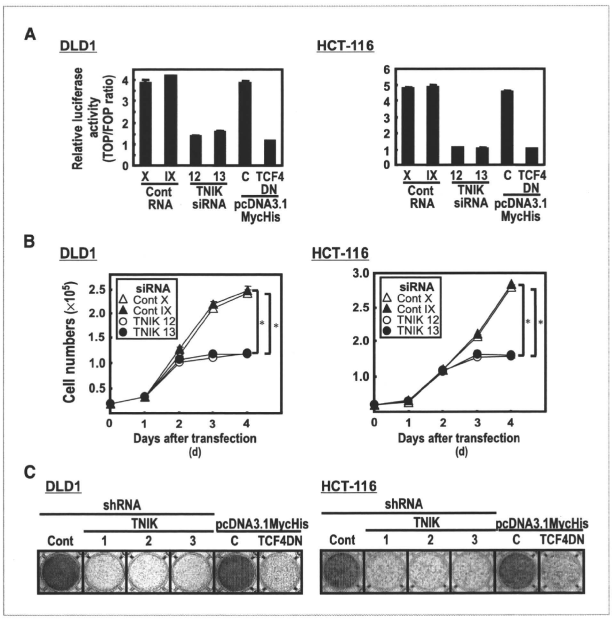

Figure 4. Inhibition of TCF/LEF transcriptional activity and colorectal cancer cell proliferation by RNA interference against TNIK. A and B, TCF/LEF transcriptional activity (A) and proliferation (B) of DLD1 or HCT-116 cells transfected with control RNA (X or IX), siRNA against TNIK (12 and 13), pcDNA3.1 MycHis-control (C), or pcDNA3.1-MycHis-TCF4DN (positive control). Constructs X and IX are GC content–matched control RNAs for siRNA constructs 12 and 13, respectively. Forty-eight hours after transfection, luciferase activities were measured (A). The numbers of living cells were counted every 24 h by trypan blue dye exclusion (B). *, $P < 0.05$ (Mann-Whitney U test); bars, SE. C, colony formation by DLD1 or HCT-116 cells transfected with shRNA [1, 2, 3, or control (Cont)], pcDNA3.1MycHis-control (C), or pcDNA3.1MycHis-TCF4DN.

Constitutive activation of the Wnt signaling pathway seems to be necessary for maintenance of the undifferentiated status and self-renewal of colorectal cancer cells (14, 42). TNIK was essential for the transcriptional activity of the TCF4 and β-catenin complex in colorectal cancer cells (Fig. 4; ref. 21). We newly observed that TNIK was essential for the continuation of colorectal cancer cell proliferation. Knockdown of TNIK by different siRNA constructs induced marked suppression of the TCF/LEF transcriptional activity and colorectal cancer cell proliferation (Fig. 4). To exclude the off-target

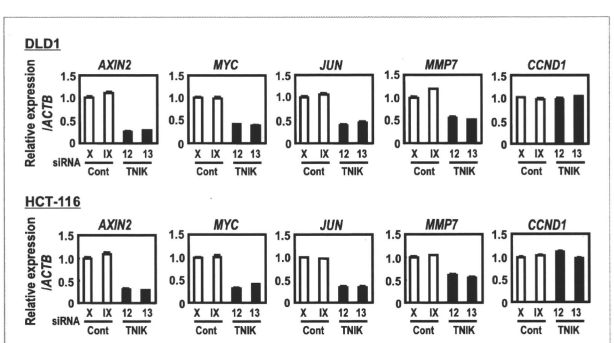

Figure 5. Regulation of TCF/LEF target gene expression by TNIK. DLD1 or HCT-116 cells were transfected with siRNA against TNIK (12 or 13) or control RNA (X or IX). Forty-eight hours after transfection, the relative expression levels of genes encoding axis inhibitor-2 (*AXIN2*), c-myc (*MYC*), c-jun (*JUN*), matrilysin (*MMP7*), and cyclin D1 (*CCND1*) were quantified by real-time reverse transcription-PCR and expressed as ratios (ΔΔCT) relative to the controls (X).